PHYSICAL REVIEW B **87**, 184204 (2013)

Loop models with crossings

Adam Nahum,[1] P. Serna,[2] A. M. Somoza,[2] and M. Ortuño[2]
[1]*Theoretical Physics, Oxford University, 1 Keble Road, Oxford OX1 3NP, United Kingdom*
[2]*Departamento de Física–CIOyN, Universidad de Murcia, Murcia 30.071, Spain*
(Received 10 March 2013; published 28 May 2013)

The universal behavior of two-dimensional loop models can change dramatically when loops are allowed to cross. We study models with crossings both analytically and with extensive Monte Carlo simulations. Our main focus (the "completely packed loop model with crossings") is a simple generalization of well-known models that shows an interesting phase diagram with continuous phase transitions of a new kind. These separate the unusual "Goldstone" phase observed previously from phases with short loops. Using mappings to $\mathbb{Z}_2$ lattice gauge theory, we show that the continuum description of the model is a replica limit of the σ model on real projective space ($\mathbb{RP}^{n-1}$). This field theory sustains $\mathbb{Z}_2$ point defects, which proliferate at the transition. In addition to studying the new critical points, we characterize the universal properties of the Goldstone phase in detail, comparing renormalization group (RG) calculations with numerical data on systems of linear size up to $L = 10^6$ at loop fugacity $n = 1$. (Very large sizes are necessary because of the logarithmic form of correlation functions and other observables.) The model is relevant to polymers on the verge of collapse, and a particular point in parameter space maps to self-avoiding trails at their Θ point; we use the RG treatment of a perturbed σ model to resolve some perplexing features in the previous literature on trails. Finally, one of the phase transitions considered here is a close analog of those in disordered electronic systems—specifically, Anderson metal-insulator transitions—and provides a simpler context in which to study the properties of these poorly understood (central-charge-zero) critical points.

DOI: 10.1103/PhysRevB.87.184204 PACS number(s): 05.50.+q, 05.20.−y, 64.60.al, 73.20.Fz

I. INTRODUCTION

It is tempting to think that two-dimensional critical phenomena are completely classified and understood, thanks to conformal field theory and other exact techniques, but this is far from true. One class of problems which remains mysterious is that containing classical loop models and models for polymers, together with models for noninteracting fermions subject to disorder. These systems are tied together by field theory descriptions with continuous replica-like symmetries (or alternatively global supersymmetries). Examples include de Gennes' mapping of polymers to the $O(N)$ model in the limit $N \to 0$, the various replica σ models for the integer quantum Hall transition and other localization problems, and the σ models describing cluster boundaries in percolation and similar soups of loops.[1–13]

Classical loop models yield the simplest examples of this class of problems, but even they are not yet fully understood. The best-studied examples are those in which the loops are forbidden from crossing; for these, a great deal is known from conformal field theory, height model mappings, exact solutions, Schramm-Loewner evolution, and numerical simulations.[14,15] But when we move away from these models the analytical techniques often cease to apply, and we may encounter new types of critical phenomena requiring new theoretical tools.

This paper considers some of the simplest two-dimensional loop models with crossings. These reveal new universality classes of, and new mechanisms for, classical critical behavior. They also provide natural models for polymers and for deterministic motion in a random environment,[16–18] which have been intensely studied but whose phase diagrams and continuum descriptions have in general not been understood. Finally, they shed light on phenomena that are important more generally for criticality in replica or supersymmetric σ models—in particular, the role of gauge symmetries and topological point defects. The latter have recently been shown also to be important for two-dimensional Anderson metal-insulator transitions.[19,20] We will return to the analogy between loop models and localization at the end of this introduction.

A key result of previous work on loops with crossings is the existence of an unusual critical phase which is absent for noncrossing loops.[10,11,16,17,21–23] It was argued by Jacobsen, Read, and Saleur[10,11] that this corresponds to the Goldstone phase of the $O(n)$ σ model, where n is the fugacity for loops. The phase exists for $n < 2$; to make sense of this regime requires a replica-like limit or a supersymmetric formulation of the field theory. Characteristic features of the Goldstone phase had previously been found in computational studies of polymers and deterministic walks in a random environment,[16,17] as well as in an integrable loop model.[21–23] The phase appears quite generically when noncrossing loop models in the so-called "dense" regime are perturbed by the addition of crossings, which in an appropriate field theory corresponds to a breaking of symmetry.[10–12]

Here, we examine a more general class of loop models with crossings. These show new continuous phase transitions separating the Goldstone phase from noncritical phases with short loops. We construct field theories for the models and pin down the universal behavior (both in the Goldstone phase and at the new critical points) using analytic calculations and extensive Monte Carlo simulations. Finally, we give a field theoretic treatment of the closely related problem of the interacting self-avoiding trail model for a polymer.

The models we study are a "completely-packed loop model with crossings" (CPLC) on the square lattice—Fig. 1 shows a configuration—and an "incompletely packed loop

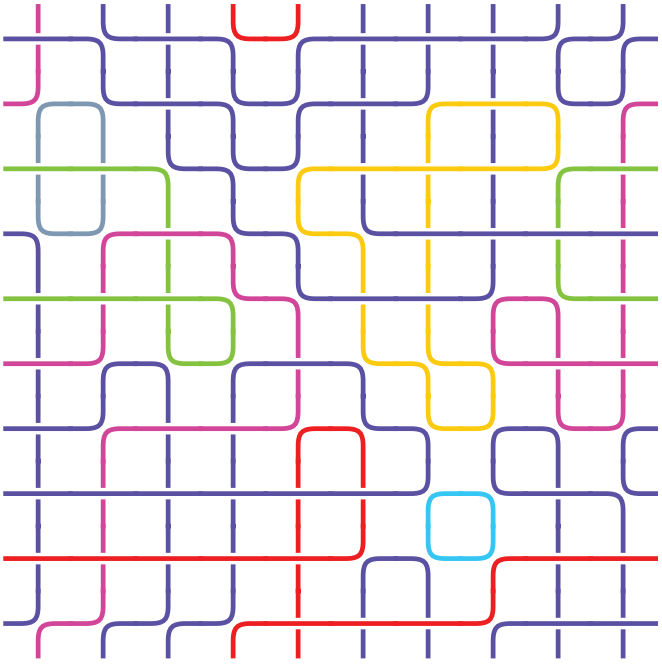

FIG. 1. (Color online) A configuration of the completely packed loop model with crossings (CPLC) on a 10×10 lattice with periodic boundary conditions. Each loop has been given a different color: these colors are merely a guide to the eye and not a part of the configuration.

model with crossings" (IPLC) in which loops are related to cluster boundaries. The parameter space for the CPLC contains various previously-studied models as special cases; in particular, the standard completely packed loop model *without* crossings and models with crossings encountered in various contexts (including those mentioned above). The CPLC and IPLC are expected to show the same universal behavior—our numerics are restricted to the CPLC, but the IPLC provides a simpler context in which to describe the main theoretical ideas.

It is easy to argue that the phase transitions in the CPLC and IPLC cannot be described by the $O(n)$ model. Instead, the general description of the models requires coupling the $O(n)$ spin $\vec{S}$ to a $\mathbb{Z}_2$ gauge field, or equivalently identifying $\vec{S}$ with $-\vec{S}$ to obtain a nematic order parameter. This leads to a σ model on a real projective space, $\mathbb{RP}^{n-1}$, in which $\mathbb{Z}_2$ point vortices play an important role. Vortices are suppressed in the Goldstone phase—meaning that the $O(n)$ model is a viable description there—but proliferate at the phase transition into the short loop phase. (This picture is appropriate for the regime $0 < n < 2$.)

In general, the introduction of crossings leads the standard exact techniques used for noncrossing loop models to fail, so for the critical points we are restricted to numerics and approximate RG treatments.[20] However, the Goldstone phase can be fully understood analytically, since it is characterized by marginal flow to a weak-coupling fixed point.[10,11] This leads to logarithms—e.g., correlation functions decaying with a universal power of the logarithm of distance—so very large system sizes are required in order to confirm our analytical predictions numerically (comparable to the largest sizes simulated in any statistical mechanics problem). These are possible at fugacity $n = 1$ thanks to special features of the problem there, and our simulations are restricted to this value.

Another feature of the CPLC at $n = 1$ is that, while each configuration is a soup of many loops, the model permits a mapping to a model for a *single* loop with local interactions. At a certain point in parameter space, this is the well-studied "interacting self-avoiding trail" (ISAT) model for a polymer at its collapse, or Θ, point.[16,24] Collapse transitions for polymers in two dimensions are a mysterious subject, which deserves clarification (see for instance the case of the missing Flory exponents.[25]) Here, we show that the ISAT can be understood completely from field theory, explaining for example the interesting phase diagram found numerically in Ref. 18. To do with we perturb the σ model that describes the Goldstone phase. Surprisingly, the Θ point of the ISAT turns out to be an *infinite order* multicritical point: despite the simplicity and naturalness of this model, it is highly fine-tuned from the point of view of general polymer models. This implies that the critical exponents for the *generic* Θ point polymer (with crossings) are still unknown.

There is a close relationship between loop models at loop fugacity $n = 1$ and disordered fermion problems.[26–32] Supersymmetry and replica-like limits, crucial in the latter for averaging over disorder, appear in the former as tools allowing geometrical correlation functions (such as the probability that two points lie on the same loop) to be expressed in field theory. Both types of problem exhibit critical points of central charge zero, described by logarithmic CFTs.[33,34] The loop models are a good place to study such critical points since they are more tractable, both analytically and computationally, than disordered fermion problems.

For completely-packed loops without crossings, there is in fact an exact mapping[26,27] to a network model for Anderson localization in symmetry class C.[7,35,36] However, the analogy is more general. Recent work by Fu and Kane[20] demonstrates that the metal-insulator transition in the symplectic symmetry class is driven by proliferation of $\mathbb{Z}_2$ vortices; this transition is thus in remarkably close analogy with those in the loop models discussed here, though the appropriate σ model is different. In the localization language, the Goldstone phase corresponds to a metallic phase, and the two short loop phases—which are distinguished from each other by the presence or absence of a loop encircling the boundary—to topological and trivial insulating phases.

The CPLC at $n = 1$ can in fact be obtained as a "classical" limit of a network model in which a Kramers doublet propagates on every edge: the above similarities show that this classical limit captures a surprising number of the qualitative features of the phase diagram for the symplectic class.

In both the loop model and the localization problem, the vortex fugacity (including its sign) plays an important role. Reference 20 introduced an approximate RG treatment of this fugacity, and in Sec. V C, we apply this to the loop models. We note that vortices—this time $\mathbb{Z}$ vortices—have also been shown to be responsible for Anderson localization in the chiral symmetry classes, and a detailed treatment has been given by König *et al.* in Ref. 19.

The organization of the paper is as follows. In the next section, we introduce the models we will study and their phase diagrams. In Sec. III, we map them to lattice gauge

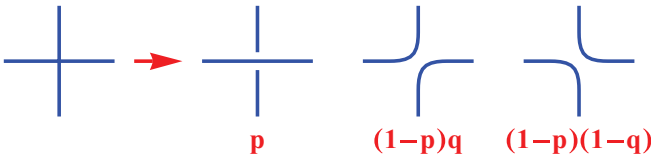

FIG. 2. (Color online) The three configurations of a node and associated Boltzmann weights. (In the leftmost configuration, the upper and lower links lie on the same loop.) The weights q and $1-q$ are exchanged on the two sublattices of the square lattice.

theories and $\mathbb{RP}^{n-1}$ σ models, paying attention to the role of topological defects and the relation to the field theory for loops without crossings. We also discuss the different ($\mathbb{CP}^{n-1}$) σ model which applies on the boundaries of the phase diagram for the CPLC. Sections IV and V apply Monte Carlo and RG calculations in the field theory to the Goldstone phase and the critical points, respectively. Our numerical methods are described in more detail in Sec. VI. Section VII tackles the polymer collapse problem. Finally, Sec. VIII discusses directions for future work.

II. DEFINITIONS OF MODELS

A. Completely packed loops with crossings

Configurations of the completely packed loop model with crossings (CPLC) are generated by resolving each node of the square lattice in one of the three possible ways shown in Fig. 2. Figure 1 shows an example on a small lattice. Note that overcrossings are not distinguished from undercrossings—the configuration at a node is defined solely by the way its four links are paired up.

Each of the three possible pairings at a node is assigned a weight, as shown in Fig. 2, with the weight of a crossing being p. The factors q and $1-q$ are staggered (swapped) on the two sublattices of the square lattice, so that the states of the system for extreme values of the parameters are as shown in Fig. 3. The Boltzmann weight for a configuration is given by the product of the node factors, together with a fugacity n for the loops. Let N_p, N_q, and N_{1-q} denote the numbers of nodes where the pairing with weight p, $(1-p)q$ or $(1-p)(1-q)$ is chosen. Then the product of node weights in a configuration $\mathcal{C}$ is

$$W_{\mathcal{C}} = p^{N_p}\,[(1-p)q]^{N_q}\,[(1-p)(1-q)]^{N_{1-q}}\,, \qquad (1)$$

and the partition function is

$$Z = \sum_{\mathcal{C}} n^{\text{no. loops}}\, W_{\mathcal{C}}. \qquad (2)$$

The parameter space of this model includes various previously investigated models. On the line $p=0$, we have the completely packed loop model *without* crossings, which has been intensely studied and which may be mapped to the n^2-state Potts model via the Fortuin-Kasteleyn representation of the latter. The model on the line $q=1/2$ was related to the Goldstone phase of the $O(n)$ σ model in Ref. 10, and points on this line have been studied in various contexts. For a given value of n, the point $q=1/2$, $p=(2-n)/(10-n)$ is known as the Brauer loop model[21–23] and is integrable; this model was related to a supersymmetric spin chain in Ref. 21. When the parameters in the CPLC are such that all configurations given equal weight—i.e., when $n=1$, $q=1/2$, and $p=1/3$—it is equivalent to a standard model for polymers at their Θ (collapse) point,[16,18,24] which we will discuss further in Sec. VII. On the lines $q=0$ or $q=1$—the left and right boundaries of the phase diagram in Fig. 3—the CPLC reduces to the "Manhattan" lattice loop model discussed in Refs. 27,37. Loop models with crossings at $n=1$ have also appeared in the study of Lorentz lattice gases, i.e., deterministic motion in a random environment.[17,38] Finally, Ref. 39 discusses a model similar to the CPLC in which q and $1-q$ are not staggered, and uses it (at $n=2$) to analyze the phase diagrams of vertex models.

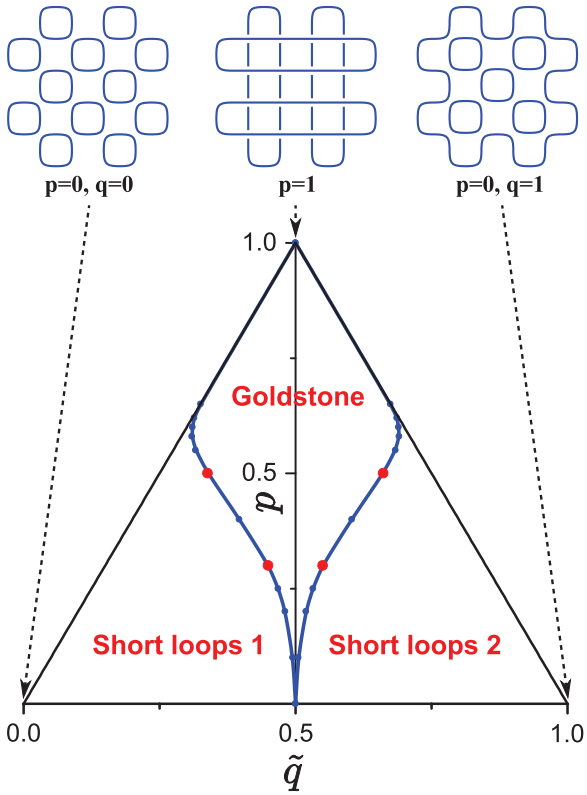

FIG. 3. (Color online) Phase diagram obtained numerically for the CPLC at $n=1$. The horizontal axis is labeled by $\tilde{q}$, defined by $(\tilde{q}-1/2)=(q-1/2)(1-p)$. The larger (red) dots on the critical line indicate the values of p at which we have analysed the critical behavior in detail. Also shown are the configurations obtaining on a small finite lattice at $p=1$, at $p=0$, $q=0$, and at $p=0$, $q=1$. (The point $p=0$, $q=1/2$ is the percolation critical point.)

A trivial but important fact about the CPLC is that the nodes become completely independent of each other when $n=1$. The weights p, $(1-p)q$, and $(1-p)(1-q)$ are then the probabilities of the various node configurations, and the partition function Z is equal to unity—from which it follows, by the finite size scaling of the free energy, that any critical points must have central charge $c=0$. The model with $n=1$ is thus analogous to percolation, which can also be formulated in terms of uncorrelated random variables. In the absence of crossings, the $n=1$ model is in fact equivalent to bond percolation on a dual lattice, with loops surrounding cluster boundaries; however when crossings are allowed the universal behavior is no longer that of percolation.

Our simulations will be restricted to the case $n = 1$, which is the most interesting and the best suited to Monte Carlo, but most analytic results will apply to $0 \leqslant n < 2$. (We will discuss the case $n = 2$, which shows more conventional critical behavior, elsewhere.) The phase diagram obtained numerically at $n = 1$ is shown in Fig. 3. We expect it to be qualitatively similar for $0 < n < 2$, with the Goldstone phase swallowing up more and more of the parameter space as $n \to 0$. We now summarize its main features.

(1) Short loop phases: the configurations at $p = 0$, $q = 0$ and at $p = 0, q = 1$ provide caricatures of the two "short loop" phases. For given boundary conditions, these are distinguished from each other by the presence or absence of a long loop running along the boundary, as shown in Fig. 3. In a σ model description, the short loop phases are massive (disordered) phases. In the analogy with Anderson localization mentioned in the Introduction, they correspond to insulating phases, and the boundary loops correspond to the edge states present in a topological insulator.

(2) Goldstone phase: in the Goldstone phase, so-called because the continuum description is a σ model which flows to weak coupling in the infra-red,[10] the loops are "almost" Brownian. However, interactions between Goldstone modes in the σ model are only marginally irrelevant, leading to universal logarithmic forms for correlators and other observables which we calculate in Sec. IV. In the Anderson localization analogy, this would be a metallic phase.

(3) Critical lines: the lines separating the Goldstone phase from the short loop phases show a new universality class of critical behavior. This is associated with the order-disorder transition of the $\mathbb{RP}^{n-1}$ σ model, which exists only in the replica limit $n < 2$ and is driven by proliferation of $\mathbb{Z}_2$ vortex defects associated with $\pi_1(\mathbb{RP}^{n-1})$ (see Secs. III and V C). Numerically, the critical loops have $d_f = 1.909(1)$ at $n = 1$, i.e., they are slightly less compact than Brownian paths, and the transition has a large correlation length exponent $\nu = 2.745(19)$ (see Sec. V).

(4) Critical point at $p = 0$: the critical point of the loop model without crossings (at $p = 0$, $q = 1/2$) is well studied and corresponds to the so-called dense phase of the $O(n)$ loop model, or to SLE_κ with $\kappa > 4$. [Note that the standard terminology "$O(n)$ loop model" is potentially misleading, as when crossings are forbidden the $O(n)$ model is not the appropriate field theory for the dense phase.[9,10]] At $n = 1$, this point maps to critical percolation; the loops have the statistics of percolation cluster boundaries, with a fractal dimension $d_f^{\mathrm{perc}} = 7/4$, and the correlation length exponent of the transition is $\nu^{\mathrm{perc}} = 4/3$. These critical exponents also yield exponents in an Anderson transition (the spin quantum Hall transition) via an exact mapping.[26–28,40]

(5) Phase diagram boundaries: everywhere on the boundary of the phase diagram in Fig. 3—i.e., whenever one of the node weights vanishes—loops can be consistently oriented by assigning a *fixed* (configuration independent) orientation to each link of the lattice. The necessary choice of orientations differs on each of the three pieces of boundary. They are those of the "L" lattice on the line $p = 0$, and of the Manhattan lattice on the lines $q = 0$ and 1. (These lattices are depicted in Ref. 27.) The fact that the loops automatically come with an orientation means that the continuum descriptions have a higher symmetry,[9,41] as will be discussed in Sec. III F, and the appropriate field theory is a σ model on complex projective space, $\mathbb{CP}^{n-1}$, rather than on $\mathbb{RP}^{n-1}$. The $\mathbb{CP}^{n-1}$ description implies that the lines $q = 0$ and 1 (the Manhattan lattice loop model) are always in the short loop phase, but with a typical loop length that diverges exponentially as $p \to 1$ (see Sec. III F). This is in agreement with previous expectations,[27,37] but is not obvious from the numerical phase diagram since the critical lines closely approach the lines $q = 0, 1$ for p close to one.

(6) Relation to polymers: configurations in the CPLC are soups of many loops. However, when $n = 1$, the CPLC has a simple relation with the self-avoiding trail model for a single polymer.[16,18] The polymer corresponds to a single marked loop in the soup of loops; so long as $n = 1$, integrating out the configurations of the other loops leads to a local Boltzmann weight for the marked one. Adding the interactions that are natural in the polymer language takes us out of the parameter space of Fig. 3, but the σ model description can be extended to cover this case by including appropriate symmetry-breaking terms (see Sec. VII).

B. Incompletely packed loops with crossings

For pedagogical reasons, it will be useful to introduce and discuss a second loop model before returning to the CPLC. Loops in the new model will no longer be completely packed, but nevertheless the universal properties will be the same. We refer to this model as the incompletely packed loop model with crossings, or IPLC.

To generate a configuration in the IPLC, we first color the plaquettes of the square lattice black or white, giving a site percolation configuration on the square lattice formed by the plaquettes. The loops in the IPLC are then cluster boundaries, as shown in Fig. 4. However, the loop configuration is not uniquely determined by the cluster configuration: for each "doubly visited" node, where two cluster boundaries meet, we must choose how to connect them up. Allowing crossings, the three possible pairings are again those of Fig. 2 (but unlike in the CPLC we do not assign different weights to the different pairings).

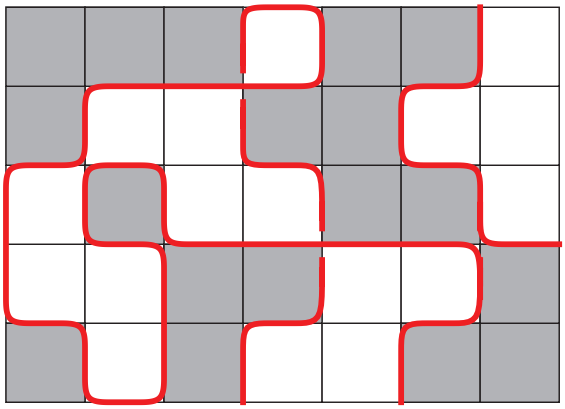

FIG. 4. (Color online) Part of a configuration in the IPLC. In this model, the loops (thick red lines) are cluster boundaries. Universal behavior in the IPLC is expected to coincide with that in the CPLC.

The simplest choice for the Boltzmann weight is to give each percolation configuration the standard percolation probability $q^B(1-q)^W$, where B and W are the numbers of black and white faces. A given percolation configuration corresponds to 3^N loop configurations, where N is the number of doubly visited nodes. Assigning them equal probability, the partition function for the IPLC is

$$Z = \sum_{\text{configs}} \alpha^N q^B (1-q)^W, \tag{3}$$

with $\alpha = 1/3$. The parameter q here will play a similar role to the parameter q in the CPLC.

The above partition function corresponds to a loop fugacity $n = 1$. We will wish to generalize it to arbitrary n. We may also vary α, and introduce a fugacity x for the total *length* of loops:

$$Z = \sum_{\mathcal{C}} \alpha^N q^B (1-q)^W x^{\text{length}} n^{\text{no. loops}}. \tag{4}$$

The precise values of α and x will not be important in what follows. When $n = 1$, a length fugacity x distinct from one corresponds to an Ising interaction of strength J between colours of adjacent squares, with $x = e^{-2J}$, and varying α introduces a four-site interaction. These interactions have no effect on the universal behavior so long as they are weak.

Note that if we take our lattice to have the topology of the disk, regarding the region outside the boundary as white for the purposes of drawing cluster boundaries, the IPLC shares with the CPLC the feature of having an edge loop at $q = 1$ but not at $q = 0$. There are clearly stable short-loop phases at small q and at q close to one, and field theory arguments lead us to expect a stable Goldstone phase near $q = 1/2$. The conjectured phase diagram, shown in Fig. 5, is similar to a slice through the phase diagram of the CPLC at some nonzero value of p. (If we had forbidden crossings, we would have obtained a phase diagram similar to the line $p = 0$ in the CPLC.)

III. LATTICE FIELD THEORIES

A. Lattice field theory for IPLC

We begin with the IPLC, which permits a simple mapping to a $\mathbb{Z}_2$ lattice gauge theory coupled to matter fields. We will first write down this theory and then show that a graphical expansion similar to the high temperature expansion of the Ising model or the Nienhuis $O(n)$ model[42,43] provides the connection to the loop model.

The required lattice field theory includes matter fields, which are real n-component vectors living on the sites i of the square lattice,

$$\vec{S}_i = \left(S_i^1, \ldots, S_i^n\right), \quad \vec{S}_i^2 = n, \tag{5}$$

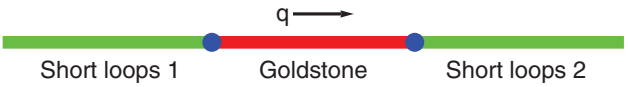

FIG. 5. (Color online) Schematic phase diagram for the incompletely packed loop model with crossings as a function of q (for fixed $n \sim 1, \alpha \sim 1/3, x \sim 1$).

and gauge fields $\sigma_{ij} = \pm 1$ living on the links. The partition function is

$$Z = \mathrm{Tr} \prod_F \left[(1-q) + q \prod_{\langle ij \rangle \in F} \sigma_{ij} \right] \prod_{\langle ij \rangle} (1 + x \sigma_{ij} \vec{S}_i \cdot \vec{S}_j). \tag{6}$$

Tr denotes sums and integrals over all degrees of freedom (σ and $\vec{S}$), normalized so $\mathrm{Tr}\, 1 = 1$, and F denotes a face (square) of the lattice. The $\mathbb{Z}_2$ gauge symmetry of this model is

$$\vec{S}_i \to \chi_i \vec{S}_i, \quad \sigma_{ij} \to \chi_i \chi_j \sigma_{ij} \quad (\text{for } \chi_i = \pm 1). \tag{7}$$

Above, we have written the Boltzmann weight for the gauge field in a form suitable for the graphical expansion. Later, we will rewrite it in a more conventional form.

The graphical expansion begins by expanding out the product over faces F and representing the terms by a simple graphical rule (a face is coloured black if the q term is chosen, and white if the $1-q$ term is chosen). This generates percolation configurations $\mathcal{P}$,

$$Z = \sum_{\mathcal{P}} q^B (1-q)^W \,\mathrm{Tr} \left(\prod_{l \in \partial \mathcal{P}} \sigma_l \right) \prod_{\langle ij \rangle} (1 + x \sigma_{ij} \vec{S}_i \cdot \vec{S}_j), \tag{8}$$

where $\partial \mathcal{P}$ denotes the set of links lying on percolation cluster boundaries.

Next we expand out the product over links. Only one term in this expansion survives after summing over σ_{ij}, namely that in which the factors of $\vec{S}_i \cdot \vec{S}_j$ lie on the cluster boundaries:

$$Z = \sum_{\mathcal{P}} q^B (1-q)^W x^{\text{length}} \,\mathrm{Tr} \prod_{\langle ij \rangle \in \partial \mathcal{P}} S_i^a S_j^a. \tag{9}$$

"Length" refers to the total length of cluster boundaries. We have written the spin index a explicitly in the inner product $\vec{S}_i \cdot \vec{S}_j$ to emphasize that each link on a cluster boundary now carries an index $a = 1, \ldots, n$. Finally, we perform the remaining integrals over the vectors $\vec{S}$, using

$$\begin{aligned} \mathrm{Tr}\, S_i^a S_i^b &= \delta^{ab}, \\ \mathrm{Tr}\, S_i^a S_i^b S_i^c S_i^d &= \frac{n}{n+2} (\delta^{ab}\delta^{cd} + \delta^{ac}\delta^{bd} + \delta^{ad}\delta^{bc}). \end{aligned} \tag{10}$$

The three terms in the second formula correspond to the three ways of connecting up the links in pairs at a node for which all four links are in $\partial \mathcal{P}$. Expanding out all such brackets gives 3^N terms, each associated with a loop configuration $\mathcal{C}$. For a given $\mathcal{C}$, each loop comes with a product of δ functions forcing the indices a to be equal for all links on that loop. We may therefore think of each loop as carrying a "color" index ranging from $1, \ldots, n$. Summing over the possible colours for each loop yields a fugacity n:

$$Z = \sum_{\mathcal{C}} \alpha^N q^B (1-q)^W x^{\text{length}} n^{\text{no. loops}}. \tag{11}$$

The parameter α is $n/(n+2)$ as a consequence of Eq. (10). It can be varied by exchanging the hard constraint $\vec{S}^2 = n$ for a potential for $\vec{S}^2$.

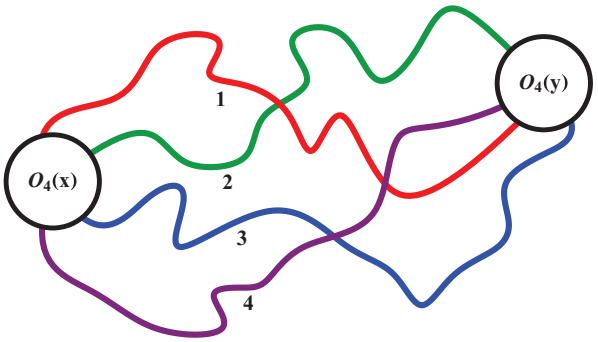

FIG. 6. (Color online) The watermelon correlator $G_4(x,y)$.

B. Correlation functions and the replica trick

We have seen that a graphical expansion of the lattice gauge theory (6) generates the configurations of the loop model with the right weights. The correspondence also extends trivially to correlation functions. Switching temporarily to a continuum notation, the basic ones are the watermelon correlation functions $G_k(x,y)$, which give the probability that k distinct strands of loop connect x and y. For example, on the lattice G_2 can be taken to be the probability that two links lie on the same loop, and G_4 the probability that two nodes are connected by four strands.

In the continuum, the correlator G_k is the two-point function of the "k-leg" operator O_k:

$$O_k(x) \propto S^1(x)S^2(x)\cdots S^k(x). \tag{12}$$

G_k vanishes for odd k, either by gauge invariance or equivalently because two regions cannot be joined by an odd number of strands (for example, if two sites lie on the same loop they are joined by two strands). We can visualize the above operator, when inserted into a correlation function, as emitting k strands with color indices ranging from 1 to k (see Fig 6).

We see that in order to write down the correlator G_k, we require the number n of spin components to be at least k. This presents a problem if the model we wish to study has a loop fugacity $n < k$: for the model of most interest to us with $n = 1$, it does not allow us to write down any of the above correlation functions! Fortunately, this problem can be resolved in two standard ways.

Firstly, we can treat $n \to 1$ as a replica-like limit, so that

$$G_k = \lim_{n\to 1} \langle O_k(x)O_k(y)\rangle . \tag{13}$$

This trick may also be used for other values of the loop fugacity, integer or noninteger. For integer n, there is a more rigorous alternative, which is to use supersymmetry.[2,3] This allows us to increase the number of components of $\vec{S}$ without increasing the loop fugacity, by making some of the components fermionic. For our purposes, the two approaches are equivalent, so for presentational simplicity we will use the replica language. The required supersymmetric construction is explained in Refs. 10 and 12: in outline, $\vec{S}$ is replaced by a vector $\vec{\Phi}$ with both bosonic and fermionic components,

$$\vec{\Phi} = (\vec{S},\vec{\eta},\vec{\xi}), \quad \vec{S}^2 + 2\vec{\eta}\cdot\vec{\xi} = n, \tag{14}$$

where $\vec{S}$ has $n+2m$ components and $\vec{\eta}$, $\vec{\xi}$ each have m anticommuting components. The loop fugacity determines n, but m is arbitrary—supersymmetry ensures that the partition function and its loop representation do not depend on it. Thus m may be chosen large enough for any desired correlator to be constructed.

C. $\mathbb{Z}_2$ vortices and $\mathbb{Z}_2$ fluxes

The local gauge-invariant degree of freedom in the lattice gauge theory (6) is a nematic vector, obtained by identifying $\vec{S}$ with $-\vec{S}$. It can be encoded in a real symmetric matrix,

$$Q^{ab} = S^a S^b - \delta^{ab}, \quad \text{tr}\, Q = 0, \tag{15}$$

which will be the relevant degree of freedom on long length scales. Q lives on real projective space, $\mathbb{RP}^{n-1}$; since this manifold has nontrivial fundamental group,[44] the Q configuration can have vortex defects which we now discuss.

$\mathbb{RP}^1$ is equivalent to the circle, so at the special value $n = 2$ vortices are standard XY vortices and are characterized by an integer topological charge. However, $\pi_1(\mathbb{RP}^{n-1}) = \mathbb{Z}_2$ when $n > 2$, so in general the vortex charge is defined only modulo two. In the replica limit—which requires analytic continuation of formulas defined for arbitrarily large n to $n < 2$—the vortices should again be viewed as $\mathbb{Z}_2$ vortices. [This may be clearer in the supersymmetric formulation of the $n = 1$ loop model, Eq. (14), where the bosonic part of the superspin lives on $\mathbb{RP}^{2m}$ for $m \geqslant 1$, which has fundamental group $\mathbb{Z}_2$.]

For a more concrete picture, we return to $\vec{S}$ and σ. Let $\sigma_l = +1$ on all links l, except for a semi-infinite string of parallel links ending at a plaquette F (see Fig. 7). The flux $\prod\sigma$ is then -1 only on F. The spin configurations which maximize the Boltzmann weight vary smoothly except at the string, across which $\vec{S}$ changes sign. This indicates the presence of a $\mathbb{Z}_2$ vortex located at F. (This connection between vortices in nematics and $\mathbb{Z}_2$ fluxes is standard.[45])

Since vortices are associated with plaquettes of nontrivial flux, we can assign a vortex number to each plaquette which is

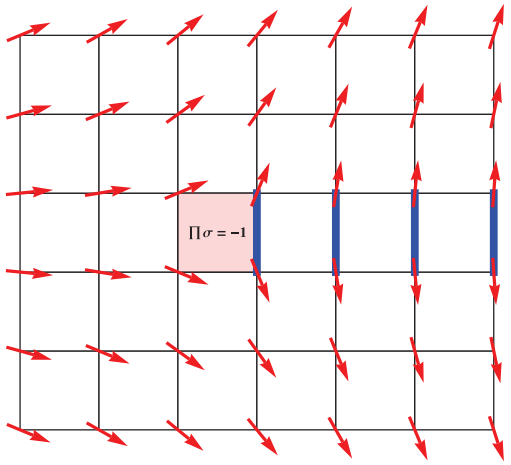

FIG. 7. (Color online) Plaquettes with gauge flux $\prod\sigma = -1$ (shaded in pink) are endpoints of strings of links with $\sigma = -1$ (marked in bold/blue), across which $\vec{S}$ changes sign. In terms of the nematic order parameter, which is obtained by identifying $\vec{S}$ with $-\vec{S}$ and which lives on $\mathbb{RP}^{n-1}$, these plaquettes are vortices. (This is of course a caricature, neglecting fluctuations.)

$+1$ if $\prod \sigma = -1$ and 0 if $\prod \sigma = 1$. The gauge field part of the Boltzmann weight can then be written in terms of the number N_v of vortices:

$$\prod_F \left[(1-q) + q \prod_{\langle ij \rangle \in F} \sigma_{ij} \right] = (1-2q)^{N_v}. \tag{16}$$

We see that the factor $(1-2q)$ is simply a fugacity for vortices, and that the exchange $q \leftrightarrow 1-q$ corresponds to changing the sign of the vortex fugacity.

This sign distinguishes the two short-loop phases in Fig. 5 from each other. In Ref. 20, $\mathbb{Z}_2$ vortices play an analogous role in a σ model for localization, with the sign of the vortex fugacity distinguishing two insulating phases. (The vortex fugacity is also important for the critical behavior[20]—see Sec. V C.)

Let us rewrite the Boltzmann weight for σ in the conventional form for $\mathbb{Z}_2$ gauge theory. In the absence of a boundary, Eq. (6) may be written as

$$Z \propto \mathrm{Tr} \exp\left(\kappa \sum_F \prod_{\langle ij \rangle \in F} \sigma_{ij} \right) \prod_{\langle ij \rangle} (1 + x\, \sigma_{ij} \vec{S}_i \cdot \vec{S}_j), \tag{17}$$

where the gauge field stiffness is

$$\kappa = \frac{1}{2} \ln \frac{1}{|1-2q|}. \tag{18}$$

In the presence of a boundary, denoted ∂, the Boltzmann weight acquires an additional term when $q > 1/2$:

$$\prod_{\langle ij \rangle \in \partial} \sigma_{ij}. \tag{19}$$

This term effects the sign change in the vortex fugacity. It is equal to $(-)^{N_{\mathrm{strings}}}$, where N_{strings} is the number of $\sigma = -1$ strings that terminate on the boundary. Since this number is equal to the number of vortices in the interior modulo 2, $(-)^{N_{\mathrm{strings}}} = (-)^{N_v}$.

We see that the sign of the vortex fugacity does not affect bulk properties. Instead, it determines the presence or absence of an edge loop.

Finally, consider the point $q = 1/2$. The vortex fugacity vanishes here [see Eq. (16)]; however, the universal properties of this point do not differ from those in the rest of the Goldstone phase (see Fig. 5). This is because vortices are anyway RG irrelevant in that phase. We discuss this in the next section in terms of a σ model for Q.

The suppression of vortices (either microscopically or in the infrared) means that in the Goldstone phase this σ model has a correspondence with the simpler $O(n)$ σ model. In the IPLC at $q = 1/2$ this correspondence holds microscopically, since the gauge field stiffness diverges there [see Eq. (18)]. This enforces $\prod \sigma = 1$ for every face F, giving $\sigma_{ij} = \chi_i \chi_j$ (so long as the lattice lives on a simply-connected manifold[46]):

$$Z \propto \sum_{\{\chi\}} \mathrm{Tr}_S \prod_{\langle ij \rangle} [1 + x\, (\chi_i \vec{S}_i) \cdot (\chi_j \vec{S}_j)]. \tag{20}$$

Changing variables to $\vec{S}' = \chi \vec{S}$ eliminates the gauge degrees of freedom from the Boltzmann weight, leaving a lattice $O(n)$ model. (Non-gauge-invariant correlators pick up factors of χ, ensuring that they vanish,[47] however, on summing over χ.) In the regime we consider, i.e., at sufficiently large x, this $O(n)$ model is expected to be described by the $O(n)$ σ model in its Goldstone phase.

D. Continuum description

The naive continuum description of the lattice field theory (6) is a σ model for Q,

$$\mathcal{L} = \frac{K}{4} \mathrm{tr}\, (\nabla Q)^2, \tag{21}$$

together with the constraint on Q following from its definition in terms of $\vec{S}$. To conform with convention, we use the normalization $\vec{S}^2 = 1$ in the continuum [rather than Eq. (5)]; then $Q^{ab} = S^a S^b - \frac{1}{n} \delta^{ab}$.

The fugacity for vortices is hidden in the ultraviolet regularization of the σ model (21). We will restore this parameter explicitly when we consider RG in the vicinity of the critical point (see Sec. V C), where vortices are crucial.

However, since the classical free energy of a pair of vortex defects is proportional to the stiffness K, they are suppressed at large K (as in the XY model at large stiffness). In the Goldstone phase, which we now discuss, K flows to large values under coarse-graining, and vortices are an irrelevant perturbation.

Nonsingular (i.e., vortex-free) configurations of Q are equivalent to nonsingular configurations of $\vec{S}$ (on a manifold of trivial topology, and up to a global sign ambiguity). Thus for a perturbative treatment at large K, the $\mathbb{RP}^{n-1}$ σ model can be replaced with the more familiar $O(n)$ σ model, argued previously[10] to apply to the CPLC at $q = 1/2$:

$$\mathcal{L} = \frac{K}{2} (\nabla \vec{S})^2, \quad \vec{S}^2 = 1. \tag{22}$$

The perturbative beta function for K changes sign at $n = 2$:[10,53]

$$\frac{\mathrm{d}K}{\mathrm{d} \ln L} = \frac{2-n}{2\pi} \left(1 + \frac{1}{2\pi K} + \cdots \right). \tag{23}$$

When $n > 2$, the stiffness flows to zero under RG and the σ model has only a disordered phase; thus the loop model is not expected to be critical. At $n = 2$, the σ model is the XY model, and we have in addition the quasi-long-range-ordered phase in which K does not flow. By the Mermin-Wagner theorem, these are the only possibilities when $n \geqslant 2$.

However, in the replica limit the Mermin-Wagner theorem does not apply,[10] and Eq. (23) shows that for $n < 2$ the stiffness K flows to infinity in the infrared. This is the Goldstone phase. At the infrared fixed point, the $n-1$ Goldstone modes are free fields, so the central charge is $c = n - 1$.[10] We now discuss the extraction of a continuum description for the CPLC, the appearance of a nontrivial vortex fugacity in that model, and the extra symmetry on the boundaries of the phase diagram.

E. Lattice field theory for the CPLC

The CPLC can again be mapped to a lattice spin model with a $\mathbb{Z}_2$ gauge symmetry, though with a less conventional form, and as long as we are in the interior of the phase diagram (see Fig. 3) the continuum description is again the $\mathbb{RP}^{n-1}$ model. The following construction is similar to that described in Ref. 13, so we give only an outline.

We again introduce fixed-length spins $\vec{S}_l$ ($\vec{S}_l^2 = n$) but for the CPLC they live on the links l of the square lattice. The Boltzmann weight involves four-spin interactions between the spins surrounding each node i:

$$Z = \mathrm{Tr}\,\exp\left(-\sum_{\text{nodes } i} E_i\right). \tag{24}$$

In order to define E_i, we denote the links surrounding i by 1,2,3,4, with the weight p pairing being 1 with 3 and 2 with 4, and the weight $(1-p)q$ pairing being 1 with 2 and 3 with 4:

$$\exp(-E_i) = p(\vec{S}_1\cdot\vec{S}_3)(\vec{S}_2\cdot\vec{S}_4) + (1-p)q(\vec{S}_1\cdot\vec{S}_2)(\vec{S}_3\cdot\vec{S}_4) + (1-p)(1-q)(\vec{S}_1\cdot\vec{S}_4)(\vec{S}_2\cdot\vec{S}_3).$$

These three terms are in correspondence with the three possibilities in Fig. 2, and a graphical expansion of the above partition function gives the sum over loop configurations defining the CPLC [see Eq. (2)].

The above Boltzmann weight again has a $\mathbb{Z}_2$ gauge symmetry: on changing the sign of the spin on the link ij, both e^{-E_i} and e^{-E_j} change sign but the overall Boltzmann weight is unchanged. The naive continuum limit is again the $\mathbb{RP}^{n-1}$ σ model described above, and the universal properties are expected to be identical with those of the IPLC. In Sec. III G, we will argue that the effective fugacity for $\mathbb{Z}_2$ vortices changes sign on the line $q = 1/2$, just as for the IPLC.

The lattice field theory (24) and the continuum limit (21) require a couple of comments. Firstly, the $\mathbb{RP}^{n-1}$ description does not apply on the boundaries of the phase diagram; here the model has a higher symmetry, which is not taken into account in (24)—see next section. Secondly, note that $\exp(-E_i)$ is not always positive. This is not an obstacle to taking the continuum limit—in fact, it is an important feature of the problem (note that non-real lattice actions are not necessarily pathological, and are the norm in quantum problems). We have seen that different signs for the vortex fugacity distinguish the two short loop phases in the IPLC, and we will see that the same is true for the CPLC. (The possibility of nonpositive Boltzmann weights can be important even in the Goldstone phase, see Sec. IV B).

In the model without crossings, discussed below, it is again crucial that the lattice Boltzmann weight is not positive since the continuum Lagrangian contains an imaginary θ term.[9] We now briefly review this formulation and discuss its implications for the phase diagram of the CPLC.

F. Phase diagram boundaries and $\mathbb{CP}^{n-1}$

As mentioned in Sec. II A, the CPLC has an additional symmetry[9,11] on the boundaries of the phase diagram (when $p = 0$, or $q = 0$, or $q = 1$). On each of the three boundaries of the phase diagram, the links of the lattice can be assigned fixed orientations, with two incoming and two outgoing links at each node, such that the allowed pairings are always between an incoming and an outgoing link. This orients all the loops. The necessary choice of link orientations differs for each of the components of the boundary, as mentioned in Sec. II A. Then instead of constructing a lattice field theory using real spins $\vec{S}$, we may take complex spins $\vec{z}$. The inner products $\vec{S}_l\cdot\vec{S}_{l'}$ in the Boltzmann weight for a given node are replaced with $\vec{z}_l^{\,\dagger}\cdot\vec{z}_{l'}$, where l is the outgoing link and l' the incoming link. One way of understanding the appearance of complex fields is to view the loops as world lines of quantum particles in $(1+1)$-dimensional space-time: the fact that we are now dealing with oriented world lines means that these particles carry a $U(1)$ charge.

The SO(n) global and $\mathbb{Z}_2$ gauge symmetry in the interior of the CPLC phase diagram are promoted to an SU(n) global and $U(1)$ gauge symmetry on its boundary. The appropriate field theory is a σ model for a field on *complex* projective space ($\mathbb{CP}^{n-1}$), with a θ term.[9,11] Complex projective space is the manifold of unit vectors $\vec{z}$ modulo the gauge equivalence $\vec{z}\sim e^{i\phi}\vec{z}$; again, a nonredundant parametrization is provided by a traceless matrix $\tilde{Q}$, which is now Hermitian rather than real symmetric ($\tilde{Q}^{ab} = z^a z^{*b} - \delta^{ab}/n$). The Lagrangian for the $\mathbb{CP}^{n-1}$ σ model is

$$\mathcal{L}_{\mathbb{CP}^{n-1}} = \frac{K}{4}\,\mathrm{tr}\,(\nabla\tilde{Q})^2 + \frac{\theta}{2\pi}\epsilon_{\mu\nu}\,\mathrm{tr}\,\tilde{Q}\nabla_\mu\tilde{Q}\nabla_\nu\tilde{Q}. \tag{25}$$

The field $\tilde{Q}$ can sustain skyrmion textures, since $\pi_2(\mathbb{CP}^{n-1}) = \mathbb{Z}$. The θ term weights skyrmions by a factor $e^{i\theta}$ and antiskyrmions by $e^{-i\theta}$. In the case $n = 2$, the above field theory is equivalent to the $O(3)$ σ model [the $O(3)$ spin is equal to $\mathrm{tr}\,\vec{\sigma}\,\tilde{Q}$, where $\vec{\sigma}$ is a vector of Pauli matrices]—for a pedagogical discussion of the θ term in this case see for example Ref. 49.

Bulk properties of the $\mathbb{CP}^{n-1}$ σ model depend on θ only modulo 2π. For $n \leqslant 2$, there is a critical point at $\theta = \pi \bmod 2\pi$; other values of θ are massive (flowing under RG to $\theta = 0 \bmod 2\pi$, $K = 0$). The critical point at $\theta = \pi$ is the critical point of the loop model at $p = 0$, $q = 1/2$.[9,11] Close to this point the bare value of θ varies as

$$(\theta - \pi) \propto (q - 1/2). \tag{26}$$

For our present purposes the $\mathbb{CP}^{n-1}$ description tells us two things. Firstly, it implies that the left- and right-hand boundaries of the phase diagram in Fig. 3, which correspond to the Manhattan lattice loop model, are localized for all p as previously expected.[27,37] Here, θ can be shown[50] to be equal to zero mod 2π, so that the σ model is in the disordered phase. However the correlation length ξ, and the typical loop size, diverge exponentially as $p \to 1$,

$$\xi \sim (1-p)^{-2} e^{\text{const.}/(1-p)} \quad (\text{when } q = 0, 1).$$

This follows from the beta function for the $\mathbb{CP}^{n-1}$ model[48] and the fact that the bare stiffness is of order $(1-p)^{-1}$. It is the behavior of ξ for noncritical localization in class C,[35] to which the Manhattan lattice loop model is related.[27]

Secondly, the $\mathbb{CP}^{n-1}$ description of the model without crossings gives a way of seeing that the vortex fugacity in the $\mathbb{RP}^{n-1}$ description of the CPLC changes sign on the central line $q = 1/2$, just as it does at the central point $q = 1/2$ in the IPLC. We now discuss this issue.

G. Vortex fugacity and the θ term for $\mathbb{CP}^{n-1}$

A natural way to approach the field theory for the CPLC, at least when the weight p for crossings is small, is by perturbing the field theory for the model without crossings.

In the $\mathbb{CP}^{n-1}$ language, making the weight p for crossings nonzero corresponds to adding a small mass for the imaginary part of $\tilde{Q}$, i.e., $\delta\mathcal{L} \propto -p\,\mathrm{tr}\,(\mathrm{Im}\,\tilde{Q})^2$.[12] This anisotropy favors real $\tilde{Q}$ and leads in the infrared to an order parameter living on $\mathbb{RP}^{n-1}$.

If we simply set $\tilde{Q}$ to be real, the kinetic term for $\mathcal{L}_{\mathbb{CP}^{n-1}}$ becomes that of $\mathcal{L}_{\mathbb{RP}^{n-1}}$, and the θ term vanishes. Thus we regain the $\mathbb{RP}^{n-1}$ σ model Lagrangian (21) for the loop model with crossings.

However, this does not mean the θ term plays no role: it vanishes only if we neglect $\mathbb{RP}^{n-1}$ vortices. In the presence of a vortex, we must allow the imaginary part of $\tilde{Q}$ to become nonzero in the vortex core, in order to retain continuity of $\tilde{Q}$ and the σ model constraint. There is then a contribution from the θ term there. This mechanism also pertains to quantum magnets described by anisotropic σ models in both $1+1$ and $2+1$ dimensions.[51,52]

The vortex core corresponds either to a half-skyrmion or to an anti-half-skyrmion, depending on the sign of the imaginary components of $\tilde{Q}$. [This can easily be visualized for $n=2$, when the perturbed $\mathbb{CP}^1$ model is equivalent to the $O(3)$ σ model with easy-plane anisotropy: a half-skyrmion corresponds to a vortex in the easy plane, with the $O(3)$ spin perpendicular to the easy plane in the core.] The effective vortex fugacity V is obtained by summing over both possibilities, half-skyrmion and anti-half-skyrmion, leading to

$$V \propto e^{i\theta/2} + e^{-i\theta/2}.$$

Since at $p=0$ we have $(\theta-\pi)\sim(q-1/2)$, the vortex fugacity in the $\mathbb{RP}^{n-1}$ description of the CPLC changes sign at $q=1/2$, just as the vortex fugacity changes sign at $q=1/2$ in the IPLC.

IV. THE GOLDSTONE PHASE

The Goldstone phase shows subtle universal behavior, different from that seen in loop models without crossings, which can however be understood in detail. Within this phase we can work with the $O(n)$ σ model,[10] as discussed in Sec. III D.

For most purposes the Lagrangian (22) will be sufficient, but to calculate the length distribution in Sec. IV C we will need to add a small perturbation, γ, which breaks the symmetry from $O(n)$ to $O(n-1)\times\mathbb{Z}_2$. Writing

$$\vec{S} = (S^1, \vec{S}_\perp), \tag{27}$$

where $\vec{S}_\perp$ is an $(n-1)$-component vector, we take

$$\mathcal{L} = \frac{K}{2}[(\nabla\vec{S})^2 + \gamma\, S_\perp^2], \quad \vec{S}^2 = 1. \tag{28}$$

We briefly recall one-loop RG results for this model,[53,56] which may be obtained easily using the background field method. $S(x)$ is decomposed into a slowly-varying field $\tilde{S}(x)$ and rapidly varying fluctuations $\phi(x)$:

$$\vec{S}(x) = \tilde{\vec{S}}(x)\sqrt{1-\phi(x)^2} + \sum_{\beta=1}^{n-1}\phi_\beta(x)\vec{e}_\beta(x). \tag{29}$$

The $e_\beta(x)$, $\beta=1,\ldots,n-1$, are a set of vectors orthogonal to $\tilde{S}(x)$ (there is a gauge freedom in this choice). If the initial UV cutoff is Λ, so that S involves modes with wave number $|k|<\Lambda$, then the modes in $\tilde{S}$ are limited to $|k|<\tilde{\Lambda}$ for the new cutoff $\tilde{\Lambda}<\Lambda$, and ϕ contains modes in the momentum shell $|k|\in(\tilde{\Lambda},\Lambda)$. Integrating ϕ out, and working to leading order in K^{-1} and γ, we obtain the RG equations

$$\frac{\mathrm{d}K}{\mathrm{d}\tau} = \frac{2-n}{2\pi}, \quad \frac{\mathrm{d}\gamma}{\mathrm{d}\tau} = \left(2 - \frac{1}{\pi K}\right)\gamma. \tag{30}$$

Here, τ is the RG time; after time τ, the new cutoff is $e^{-\tau}\Lambda$. Again, the important point is that K flows to large values in the infrared if $n<2$.[10]

Note that in two dimensions, the higher-order anisotropies (higher powers of $S_\perp^2$) are as relevant as $S_\perp^2$ at tree level, but less relevant at one-loop order. They will be important for the polymer phase diagram discussed in Sec. VII.

We now calculate a range of observables both analytically and numerically; details of the numerical procedure are given in Sec. VI. As we discuss in Sec. VII, incompatible hypotheses about the universal behavior at the point $n=1$, $p=1/3$, $q=1/2$ have previously been put forward, which is one reason for making a careful comparison of numerics and theory in the Goldstone phase.

A. Correlation functions

The watermelon correlation function $G_k(r)$ may be expressed as the two-point function of the operator $S^1\ldots S^k(x)$ (see Sec. III B). Including the UV cutoff Λ and the σ model stiffness K explicitly in the argument of G_k, a simple calculation following[53] gives

$$G_k(r\Lambda, K) = \frac{G_k\left(1, K + \frac{2-n}{2\pi}\ln\Lambda r\right)}{\left(1+\frac{2-n}{2\pi K}\ln\Lambda r\right)^{\alpha_k}}, \tag{31}$$

where the exponent in the denominator depends on k and on the loop fugacity n:

$$\alpha_k = \frac{k\,(k+n-2)}{2-n}. \tag{32}$$

The correlation function in the numerator of Eq. (31), which is evaluated at a separation of the order of the new UV cutoff, tends to a constant for large r. Thus the asymptotic behavior of the watermelon correlation functions $G_k(r)$ is given by a universal power of $\ln r$:

$$G_k(r) = \frac{C_k}{(\ln r/r_0)^{\alpha_k}}, \quad r_0 = \Lambda^{-1}e^{-\frac{2\pi K}{2-n}}, \tag{33}$$

with nonuniversal C_k, r_0.

It is interesting to note that although the stiffness K flows to infinity in the Goldstone phase—which we would usually think of as implying long range order—*all* the correlation functions G_{2l} decay to zero at large distances for $n>0$. Correlators G_k with odd k have no meaning in the $\mathbb{RP}^{n-1}$ σ model or in the CPLC but can be defined in loop models described by the $O(n)$ σ model without a $\mathbb{Z}_2$ gauge symmetry; such models allow operators that insert dangling ends. For $n=1$, G_1 tends to a constant, indicating that the entropic force between the ends of an *open* strand inserted into such a soup of closed loops vanishes at large separations.

We may contrast this with the case $n=0$, which describes the universality class of the dense polymer with crossings[10]—a

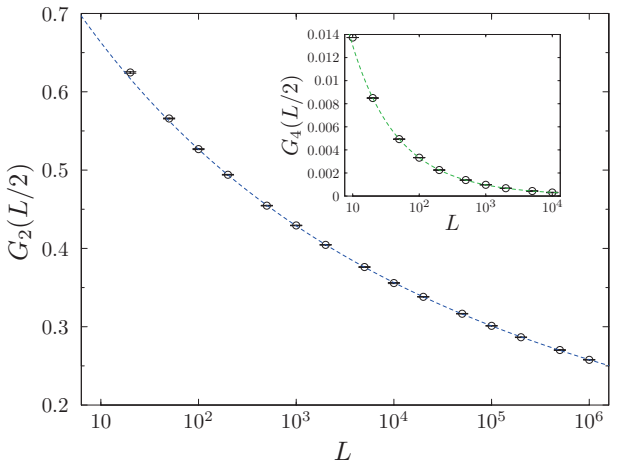

FIG. 8. (Color online) Two- and four-leg watermelon correlation functions G_2 and G_4 in the Goldstone phase. The fits are to the form $G_k = \tilde{C}_k(\ln L/r_k)^{\tilde{\alpha}_k}$ ($k = 2,4$), see text.

single loop whose length is comparable with the number of lattice sites. Here, $G_2(x)$ is a constant at large separations, in consequence of this fact. On the other hand $G_1(x)$ has a *negative* exponent α_1, indicating that if the polymer is an open strand the two ends suffer a weak entropic repulsion.

We might have expected the logarithmic form of Eq. (33) to prevent us from seeing the universal exponents α_k numerically, but this is not the case. Figure 8 shows $G_2(L/2)$ and $G_4(L/2)$ for $L \times L$ systems with periodic boundary conditions, with L ranging up to $L = 10^6$ for G_2 and $L = 10^4$ for G_4 (see Sec. VI for further details). Simulations are at $p = q = 1/2$. We fit G_2 and G_4 to the form $G_k = \tilde{C}_k(\ln L/r_k)^{-\tilde{\alpha}_k}$, leading to exponents consistent with Eq. (32):

$$\tilde{\alpha}_2 = 1.9(1), \quad \tilde{\alpha}_4 = 12.5(10). \tag{34}$$

We have $\ln r_2 = -15.4(14)$, $\ln r_4 = -18(2)$, consistent with the fact that r_0 is shared between different G_k in Eq. (33).

B. Spanning number

The logarithmic RG flow of the σ model stiffness K can be seen empirically: this stiffness is directly related to the mean "spanning number" for an $L \times L$ cylinder on which curves are allowed to terminate on the boundary. This is the number n_s of curves that traverse the cylinder from one boundary to the other. Note that n_s must be even if L is even and odd if L is odd.

To calculate n_s, the correspondence of Sec. III E between the loop model and a spin model must be extended to the case with dangling boundary links. We simply take the spins on the dangling links to be fixed, with

$$\frac{\vec{S}_{\text{top}}}{\sqrt{n}} = (\cos\theta, \sin\theta, 0, \ldots, 0), \quad \frac{\vec{S}_{\text{bottom}}}{\sqrt{n}} = (1, 0, \ldots, 0)$$

on the top and bottom boundaries (above we temporarily revert to the lattice normalization of $\vec{S}$). The graphical expansion then goes through as before, except that spanning curves acquire an additional weight $\cos\theta$.[54]

Denoting the partition function with the above boundary conditions by $Z(\theta)$, we therefore have

$$\langle(\cos\theta)^{n_s}\rangle = \frac{Z(\theta)}{Z(0)}. \tag{35}$$

In the Goldstone phase, the stiffness flows to large values in the infrared, so to calculate the right-hand side we need to consider only classical solutions with the appropriate boundary conditions. Letting x be the coordinate along the cylinder, these are

$$\vec{S} = \pm(\cos\phi(x), \sin\phi(x), 0, \ldots, 0), \quad \phi(x) = \frac{x(\theta + \pi m)}{L}.$$

Both odd and even values of m are allowed—the boundary condition is satisfied only up to a sign—but when L and m are both odd the Boltzmann weight acquires an additional minus sign, as can be seen from the lattice partition function.[55]

The action of these solutions is calculated using the renormalized stiffness $\widetilde{K}$ on scale L, leading to

$$\langle(\cos\theta)^{n_s}\rangle \simeq \sum_m (-)^{mL} \exp\left[-\frac{\widetilde{K}}{2}(\theta - \pi m)^2\right]. \tag{36}$$

For a given value of θ, only one or two values of m are not exponentially small in $\widetilde{K}$.

To extract low-order cumulants for n_s, we set $\cos\theta = e^{-x}$ and expand in x. Since expression (36) is dominated by the $m = 0$ term for $\theta \sim 0$, the difference between even and odd L is not seen. The lth cumulant is given by

$$\langle\langle n_s^l \rangle\rangle \simeq -\frac{\widetilde{K}}{2}\partial_y^l (\arccos e^y)^2\big|_{y=0}.$$

In particular, the mean spanning number is given by the renormalized stiffness $\widetilde{K}$, so

$$\langle n_s\rangle \sim \frac{2-n}{2\pi}\ln\frac{L}{L_0}. \tag{37}$$

This logarithmic flow (for $n = 1$) is seen in Fig. 9 for two points in the Goldstone phase. We have fitted the data for large sizes to the slightly more accurate form $\langle n_s\rangle \simeq \frac{1}{2\pi}(\ln L/L_0 + \ln\ln L/L_0)$, which comes from including the subleading $O(1/K)$ term in the beta function for the stiffness (23). In the upper inset to Fig. 9, we plot the numerical value of the slope $\mathrm{d}\langle n_s\rangle/\mathrm{d}\ln L$, which is seen to converge slowly to $1/2\pi$ for large L.

Since all cumulants are proportional to $\widetilde{K}$, their ratios are universal numbers that we can compare with data:

$$\langle\langle n_s^2\rangle\rangle = \frac{2}{3}\langle n_s\rangle, \quad \langle\langle n_s^3\rangle\rangle = \frac{4}{15}\langle n_s\rangle.$$

These relations are obeyed to good accuracy—plotting the two cumulants above against $\langle n_s\rangle$ for $p = 1/2$ and various L gives straight lines with slopes 0.668(5) and 0.274(18), respectively (data not shown). Note that the scaling of the cumulants means that when $\langle n_s\rangle$ becomes very large the probability distribution P_{n_s} for the spanning number becomes Gaussian (away from its tails).

To extract the probability distribution for small integer n_s, we set $\cos\theta = \epsilon$ in Eq. (36),

$$\sum_{n_s} P_{n_s}\epsilon^{n_s} \simeq e^{-\frac{\widetilde{K}}{2}(\arccos\epsilon)^2} + (-)^L e^{-\frac{\widetilde{K}}{2}(\arccos\epsilon-\pi)^2}. \tag{38}$$

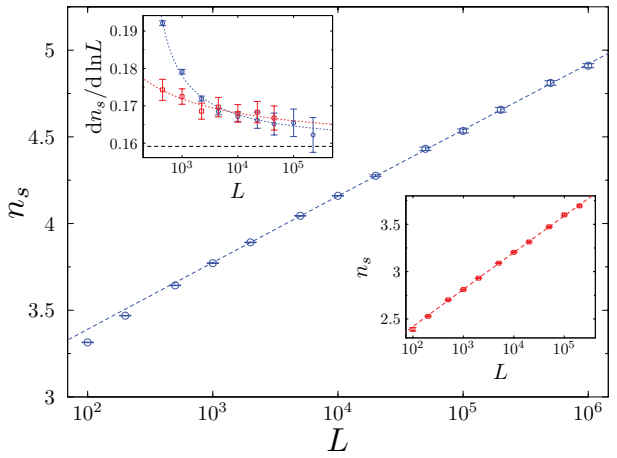

FIG. 9. (Color online) The logarithmic increase of the mean spanning number $\langle n_s \rangle$ with system size in the Goldstone phase. Main panel: $p = 1/2$, $q = 1/2$; lower inset: $p = 1/3$, $q = 1/2$. Fits are to $\frac{1}{2\pi}(\ln L/L_0 + \ln\ln L/L_0)$ with $\ln L_0 \simeq -13.78$, -8.06 for $p = 1/2$ and $1/3$, respectively. Upper inset shows the numerical estimates for the slopes $\mathrm{d}\langle n_s \rangle / \mathrm{d}\ln L$ plotted against $\ln L$—they are expected to converge to $1/2\pi$ (horizontal line).

For even circumference, this gives for example

$$P_0 = 2e^{-\pi^2\langle n_s\rangle/8}, \quad P_2 = \frac{\pi^2\langle n_s\rangle^2 - 4\langle n_s\rangle}{4} e^{-\pi^2\langle n_s\rangle/8}.$$

In Fig. 10, the expressions for $P_0, \ldots, P_8$ are compared with data (at $p = q = 1/2$ and L in the range 10^2–10^6) showing remarkable agreement. There is no free parameter in these fits.

C. Length distribution

To calculate the length distribution for a loop, we must consider the RG flow away from the Goldstone phase induced by a symmetry-breaking perturbation. To summarize the result of the following calculation, which is for $n = 1$, the probability for a loop randomly chosen from the soup to have length l falls

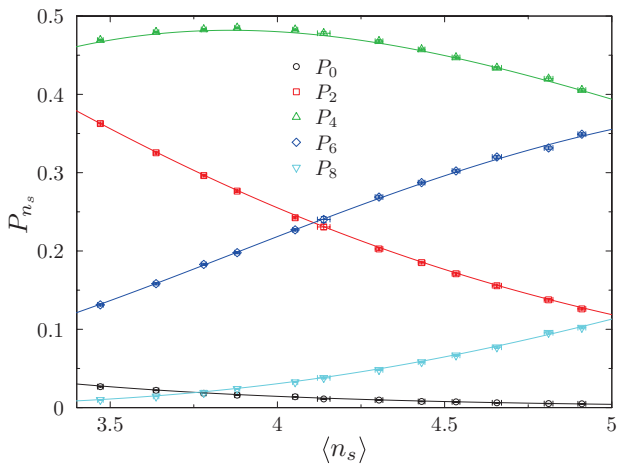

FIG. 10. (Color online) Probabilities P_{n_s} of n_s spanning curves, as a function of $\langle n_s \rangle$ (data for $p = q = 1/2$). Curves are the analytical expressions from Eq. (38), with $\widetilde{K} = \langle n_s \rangle$.

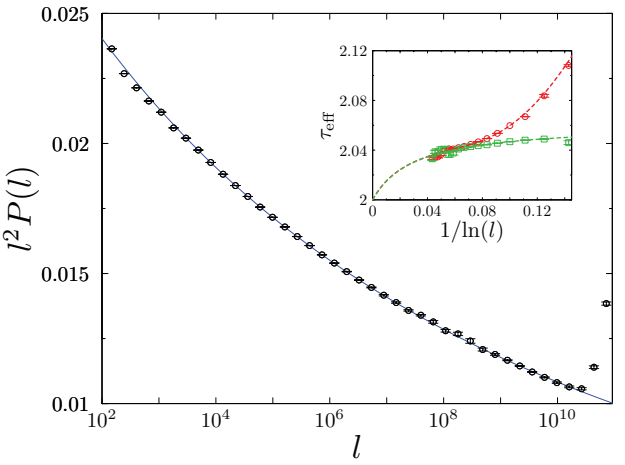

FIG. 11. (Color online) The probability distribution $P(l)$ for the length of a loop in the Goldstone phase. We have multiplied by l^2 to remove the expected power-law part, leaving the logarithmic dependence. The fit is as described in the text, with $\ln l_0 = -33.7(8)$. Data are for $p = q = 1/2$. (Inset) Two ways of defining the effective finite-size exponent value τ_{eff} (see text). Green squares are the data from $P(l)$, together with the fit (dashed line) implied by Eq. (39) ($\ln l_0 = -32.7$). Red circles are the data from $\Delta X(l)$.

off as

$$P(l) \propto \frac{1}{l^2 \ln^2(l/l_0)} \tag{39}$$

for large l.

Figure 11 shows the distribution obtained numerically for loops of length up to $l \sim 10^{10}$. We multiply $P(l)$ by l^2 in order to expose the logarithmic correction, which we fit to the form $a(\ln l/l_0)^{-c}$. We obtain

$$c = 2.03(3) \tag{40}$$

in striking agreement with Eq. (39). This value is also in agreement with numerical results for trails,[16,17] as we will discuss shortly.

Note that $P(l)$ differs by a factor of l from the length distribution for the loop passing through a fixed link,

$$P_{\text{fixed link}}(l) \propto l\, P(l), \tag{41}$$

simply because longer loops visit more links. Thus $\langle l \rangle$ evaluated using $P(l)$ is finite, as for Eq. (39).

Let $g(x)$ denote the generating function for the length of a loop randomly chosen from the soup (the "marked" loop):

$$g(x) = \sum_l P(l) x^l = \langle x^{\text{length of marked loop}} \rangle. \tag{42}$$

In order to extract $g(x)$ we use the trick of Ref. 57, splitting the components of $\vec{S}$, or equivalently the loop colours, into two groups. For simplicity, we will consider only the loop model at fugacity one, though it would be easy to generalize. We split $\vec{S}$ as in Eq. (27), yielding an $(n-1)$-component vector $\vec{S}_\perp$. In the graphical expansion of a lattice model, say of the CPLC (the IPLC would be similar), we correspondingly split the loops into unmarked loops, whose color index is equal to one, and marked loops, whose color index runs over $2, \ldots, n$. After summing over loop colors, a configuration with N marked

loops has a weight $(n-1)^N$, and expanding the partition function in $(n-1)$ is equivalent to expanding in the number of marked loops in the configuration. Writing $n' = n-1$,

$$Z(n') = \sum_{\mathcal{C}} W_{\mathcal{C}} + n' \sum_{\substack{\mathcal{C};\text{ one}\\ \text{marked loop}}} W_{\mathcal{C}} + \cdots . \tag{43}$$

Here, $W_{\mathcal{C}}$ is the weight of a configuration $\mathcal{C}$ in the CPLC at $n=1$ [see Eq. (1)]. The first term on the right-hand side is equal to one.

Next, we wish to modify the weight of a configuration by the factor x^l, where l is the total length of marked loops. This is easily done: all the inner products $\vec{S}_l \cdot \vec{S}_{l'}$ appearing in the node factors e^{-E_i} (see Sec. III E) are replaced according to

$$\vec{S}_l \cdot \vec{S}_{l'} \longrightarrow S^1_l S^1_{l'} + x\, \vec{S}_{l\perp} \cdot \vec{S}_{l'\perp}. \tag{44}$$

In this way, every unit length of marked loop picks up a factor of x, and the graphical expansion yields

$$Z(n',x) = 1 + n' \sum_{\substack{\mathcal{C};\text{ one}\\ \text{marked loop}}} W_{\mathcal{C}}\, x^l + \cdots . \tag{45}$$

Differentiating with respect to n' gives the required generating function:

$$g(x) = \frac{\partial_{n'} Z(n',x)|_{n'=0}}{\partial_{n'} Z(n',1)|_{n'=0}}. \tag{46}$$

In terms of the free energy density $f(n',x)$,

$$Z(n',x) = e^{-L^2 f(n',x)}, \quad f(n',x) = f_0 + n' f_1(x) + \cdots ,$$

this is $g(x) = f_1(x)/f_1(1)$. In order to calculate the length distribution for large values of l, we require the free energy for $x \simeq 1$ and to first order in n'.

In the continuum description, the symmetry-breaking perturbation $x \neq 1$ leads to an infinite number of relevant perturbations of which the most relevant is that in Eq. (28). Setting $x = \exp(-\mu)$ with $\mu \ll 1$, we have $\gamma \sim \mu$, the constant of proportionality being nonuniversal.

Beginning with the Lagrangian (28), we integrate out high-frequency modes, retaining their contribution to the free energy, up to an RG time τ_*. This gives

$$f(K,\gamma) = f^<(K,\gamma) + f^>(K,\gamma), \tag{47}$$

where we have split up the contribution from the modes that have been integrated out,

$$f^<(K,\gamma) = \frac{n'}{4\pi} \int_0^{\tau_*} \frac{\mathrm{d}\tau}{e^{2\tau}} \left[\ln K(\tau) + \gamma(\tau)\right] - n' A$$

[the nonuniversal constant A ensures $f < 0$, as required by Eq. (45)] and those remaining:

$$f^>(K,\gamma) = e^{-2\tau_*} f(K(\tau_*),\gamma(\tau_*)).$$

The solutions to the RG equations (30) are

$$K(\tau) = K + \frac{\tau}{2\pi}, \quad \gamma(\tau) = \gamma e^{2\tau} \left(\frac{2\pi K}{2\pi K + \tau}\right)^2 . \tag{48}$$

Stopping the RG when γ_* becomes of order one, $f^>$ may be approximated as the free energy of a massive theory in which $\vec{S}$ executes only small fluctuations around $\vec{S} = (1,0,\ldots,0)$:

$$\mathcal{L} = \frac{K_*}{2}[(\nabla \vec{S}_\perp)^2 + \gamma_* \vec{S}_\perp^2 + O(\vec{S}_\perp^4, \vec{S}_\perp^2/K_*)]. \tag{49}$$

[The $O(\vec{S}_\perp^2/K_*)$ term comes from the σ model measure.] However, the dominant terms in f come from $f^<$. To the order we require

$$f(K,\gamma) = -B + \gamma \left(2\pi K - \frac{8\pi^2 K^2}{\ln 1/\gamma} + \cdots\right) \tag{50}$$

(B is a constant). We thus have the form of the generating function at small μ:

$$\langle e^{-\mu l}\rangle = 1 - C\,\mu \left(1 - \frac{4\pi K}{\ln 1/\mu} + \cdots\right). \tag{51}$$

The constants C and K are nonuniversal, and the fact that the leading μ dependence is linear in μ is simply a consequence of the fact that $\langle l\rangle$ is finite. However, we may infer the behavior of $P(l)$ at large l from the form of the nonanalytic term, yielding Eq. (39).

Previous work on self-avoiding trails,[16,17] which map to the $n=1$ loop model at $p=1/3$, $q=1/2$ (see Sec. VII), considered a probability $Q(l)$ that may be written

$$Q(l) = \int_l^\infty P_{\text{fixed link}}(l')\mathrm{d}l'. \tag{52}$$

Viewing the loops as the trajectories of walkers, $Q(l)$ is the probability that a walker has not yet returned to its starting point after l steps. Equations (39), (41), and (52) give $Q(l) \sim 1/\ln l$. This agrees with the scaling found numerically in Refs. 16 and 17.

For a generic critical loop ensemble, $P(l) \sim l^{-\tau}$ for some $\tau \geqslant 2$, and the mean size ΔX of a loop scales with its length as $\Delta X \sim l^{1/d_f}$. The fractal dimension d_f is related to τ by

$$\tau = 2/d_f + 1. \tag{53}$$

In the Goldstone phase, $\tau = d_{\text{eff}} = 2$, with logarithmic corrections. We may define finite size estimates of τ either using $\mathrm{d}\ln P/\mathrm{d}\ln l$ or using $\mathrm{d}\ln \Delta X/\mathrm{d}\ln l$ and the scaling relation. These are plotted in the inset to Fig. 11; both are expected to converge to two, but with different logarithmic corrections.

Here, ΔX is defined as the mean extent of a loop in one of the coordinate directions. A similar quantity—the mean square end to end distance of an open trail in the ISAT model—was considered numerically by Owczarek and Prellberg,[16] and logarithmic corrections to Brownian scaling were found. It would be interesting to calculate these quantities analytically.

V. THE CRITICAL LINES

The critical lines separate the Goldstone phase from phases with short loops. In the language of the $\mathbb{RP}^{n-1}$ model, they correspond to order-disorder transitions at which $\mathbb{Z}_2$ vortices are set free. In this section we give numerically determined critical exponents for this transition at $n=1$ and briefly consider an approximate RG treatment of vortices.[19,20]

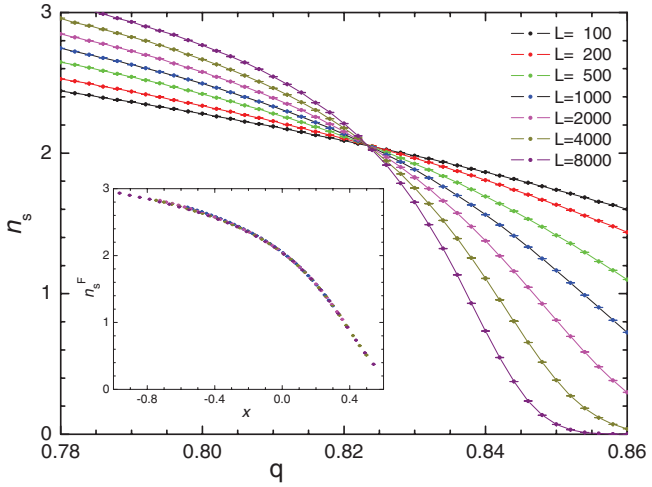

FIG. 12. (Color online) The mean spanning number n_s as a function of q for $p = 1/2$ and various system sizes, showing a crossing at the transition. (Inset) Data collapsed according to Eqs. (55) and (56).

A. Critical spanning number, ν, and $y_{\rm irr}$

At the critical point, the dimensionless quantity n_s (defined in Sec. IV B) is expected to take a universal value. This is manifested in the crossings of the various curves in Fig. 12, which shows the spanning number n_s as a function of q for $p = 1/2$ and for cylinders of various sizes. Figure 13 shows the same quantity, but in the immediate vicinity of the critical point and including much larger system sizes (up to $L = 128\,000$). The main panel of Fig. 14 shows data for $p = 0.3$; here finite size effects—visible in the drift in crossings—are much stronger.

The basic finite size scaling form for n_s is

$$n_s = h(x), \quad x = L^{1/\nu}\delta q, \tag{54}$$

where $\delta q = q - q_c$. We take into account also nonlinear dependence of the scaling variable x on δq, replacing the

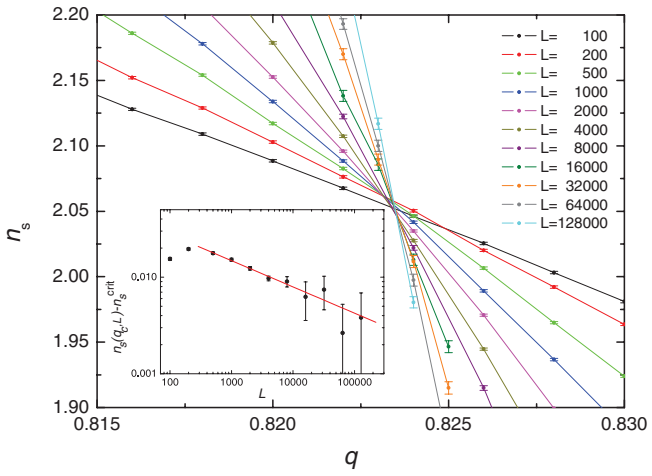

FIG. 13. (Color online) The behavior of the mean spanning number at $p = 1/2$ very close to the critical point. Note the larger system sizes compared to Fig. 12. (Inset) Finite size corrections to the spanning number at the critical point (note log-log scale) and linear fit leading to estimate of $y_{\rm irr}$.

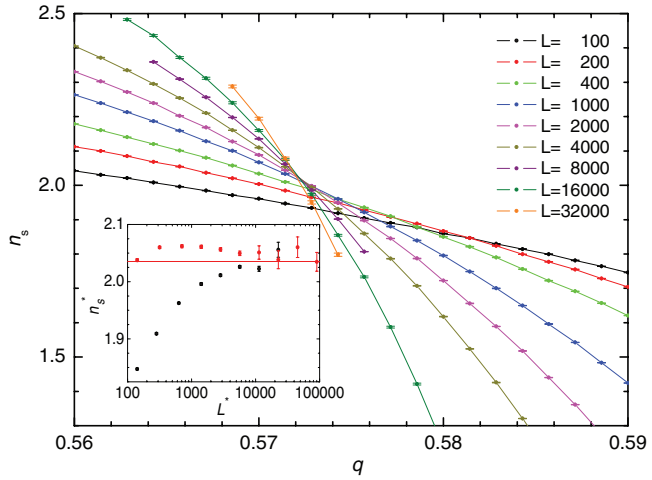

FIG. 14. (Color online) Spanning number at $p = 0.3$ (close-up of the critical point) showing larger drift in crossing points than at $p = 1/2$ (however, note different scale). (Inset) The vertical coordinate n_s^* is the crossing in the spanning number between consecutive system sizes and L^* is the geometrical mean of the sizes. Red and black dots correspond to $p = 1/2$ and $p = 0.3$, respectively. The horizontal line is the estimated asymptotic value (57).

second equation above with

$$x = L^{1/\nu}\delta q(1 + \beta_1\delta q + \beta_2\delta q^2), \tag{55}$$

and finite size corrections with (negative) irrelevant exponent $y_{\rm irr}$ in the form

$$n_s = h(x)[1 + L^{y_{\rm irr}}(\beta_3 + \beta_4 x)]. \tag{56}$$

A reasonable scaling collapse may be obtained by adjusting the values of q_c, β_i, ν, and $y_{\rm irr}$. To find these values we fit n_s to the form (56), constructing $h(x)$ using B-splines with 22 degrees of freedom. The result for $p = 1/2$ is shown in the inset to Fig. 12. What is plotted is $n_s^F = n_s/[1 + L^{y_{\rm irr}}(\beta_3 + \beta_4 x)]$, which should be equal to the scaling function $h(x)$ by Eq. (56).

Our estimates of the correlation length exponent and (universal) critical spanning number, obtained from the data at $p = 1/2$, are

$$\nu = 2.745(19), \quad n_s^{\rm crit} = 2.035(10). \tag{57}$$

We cannot constrain the irrelevant exponent very precisely. From the full fit, we obtain

$$y_{\rm irr} \in -(0.2, 0.35). \tag{58}$$

A direct estimate from the finite size corrections to the spanning number at the critical point gives a result compatible with this: the fit in the inset to Fig. 13 corresponds to $y_{\rm irr} = -0.272$.

Results for $p = 0.3$ are consistent with our expectation that all points on the critical line are in the same universality class, but error bars are larger because of larger finite size effects and smaller system sizes. We find $\nu = 2.87(10)$ and $n_s^{\rm crit} = 2.07(3)$. With regard to the convergence to a common $n_s^{\rm crit}$, see the inset to Fig. 14, which shows the vertical coordinates of the crossings between curves for consecutive L values.

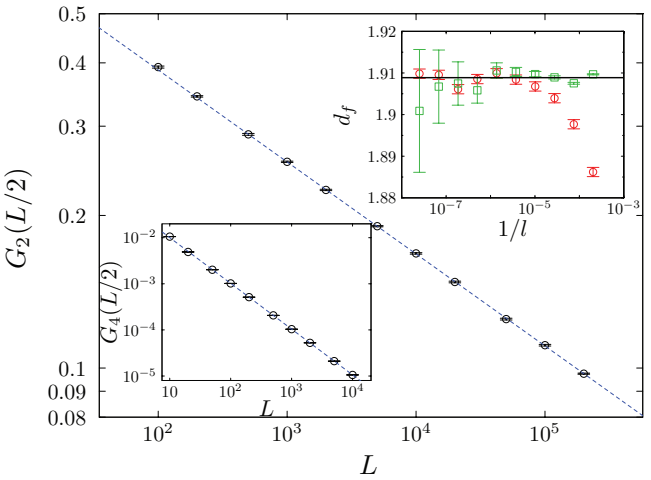

FIG. 15. (Color online) Two-leg watermelon correlator G_2 at the critical point. The power-law decay $G_2 \sim L^{-2x_2}$ gives the fractal dimension d_f via (61). The upper inset compares this value (indicated by the horizontal black line) with the finite-size estimates coming from $\Delta X(l)$ (red circles) and $P(l)$ (green squares)—see text. The lower inset shows the four-leg watermelon correlator G_4.

B. Watermelon correlators, fractal dimension, and length distribution

Next we consider the watermelon correlation functions G_2 and G_4 defined in Sec. III B. We evaluate these correlators at separation $L/2$ for a range of system sizes L—see Fig. 15. The data are for the critical point at $p = 1/2$.

Fitting to pure power laws,

$$G_k(L/2) \propto L^{-2x_k}, \tag{59}$$

we obtain the scaling dimensions of the two- and four-leg operators:

$$x_2 = 0.091(1), \quad x_4 = 0.491(1). \tag{60}$$

The scaling relation

$$d_f = 2 - x_2 \tag{61}$$

gives the fractal dimension of the critical loops,

$$d_f = 1.909(1). \tag{62}$$

We may obtain independent estimates of d_f from $\Delta X(l)$, the mean linear size of a loop of length l, and from the length distribution $P(l)$ and the scaling relation (53). The finite size estimates for d_f coming from the numerical estimates of $\mathrm{d}\ln \Delta X/\mathrm{d}\ln l$ and $\mathrm{d}\ln P(l)/\mathrm{d}\ln l$ are shown in the inset to Fig. 15. Both plots are consistent with Eq. (62).

C. RG equations in the presence of vortices

For an approximate description of the transition, we extend the RG description (23) to take account of the nonzero fugacity for $\mathbb{Z}_2$ vortices. In this, we follow the treatment by Fu and Kane of the $O(2N)/O(N) \times O(N)$ σ model at $N \to 0$.[20] This σ model and the $\mathbb{RP}^{n-1}$ σ model are similar—both sustain $\mathbb{Z}_2$ vortices, and each reduces to the XY model in an appropriate limit, which can be expanded around. An expansion around the XY limit was also considered for the $O(n)$ model near $n = 2$ in Ref. 59. The importance of topological defects in replica σ models for localization in two dimensions was also pointed out by Konig *et al.*, who developed an RG approach to localization in the chiral symmetry classes taking account of $\mathbb{Z}$ vortices.[19]

Since $\mathbb{RP}^1 = S^1$, our σ model coincides with the XY model at $n = 2$. With the normalization of Eq. (21), this has a Kosterlitz Thouless transition at the critical stiffness $K_c = 8/\pi$. The RG flow near this point is governed by the Kosterlitz RG equations for K and the vortex fugacity, which we denote V.

We assume that we can expand the RG equations in $(2 - n)$ and that V should be interpreted as the fugacity for $\mathbb{Z}_2$ vortices[58] when $n \neq 2$. At lowest order, these equations are corrected by the β-function for K in the absence of vortices, $\mathrm{d}K/\mathrm{d}\tau \simeq (2 - n)f(K)$:

$$\frac{\mathrm{d}V}{\mathrm{d}\tau} = \left(2 - \frac{\pi K}{4}\right) V, \tag{63}$$

$$\frac{\mathrm{d}K}{\mathrm{d}\tau} = (2 - n)f(K_c) - V^2. \tag{64}$$

These equations yield critical points at $K = K_c = 8/\pi$ and $V = \pm\sqrt{(2 - n)f(K_c)}$, with critical exponents

$$\nu = \sqrt{\frac{2}{(2 - n)\pi f(K_c)}}, \quad y_{\mathrm{irr}} = -\sqrt{\frac{(2 - n)\pi f(K_c)}{2}}.$$

The critical stiffness $K_c \sim 2.4$ is of roughly the same magnitude as the critical winding number $n_s^{\mathrm{crit}} \sim 2.0$ at $n = 1$ (57), as we expect from Sec. IV B. Making the further approximation of evaluating $f(K_c)$ using the perturbative β function at large K,

$$f(K) \simeq \frac{1}{2\pi}\left(1 + \frac{1}{2\pi K}\right),$$

yields at $n = 1$,

$$\nu \sim 1.9, \quad y_{\mathrm{irr}} \sim -0.5.$$

As $n \to 2$, ν diverges and the irrelevant exponent tends to zero.

As expected, this crude approximation does not give quantitatively accurate results for $n = 1$, but it does reproduce the qualitative structure of the phase diagram, with the Goldstone phase sandwiched between massive phases at positive and negative V, and the appearance of a large correlation length exponent.

A comparison with alternative approaches—for example, an approximate treatment of σ model directly at $n = 1$ in the supersymmetric formulation, or an expansion in $(2 - n)$ avoiding the additional large K approximation required here—would be desirable.

VI. NUMERICAL METHODS

We have considered system sizes from $L = 100$ up to $L = 10^6$. For sizes up to $L \sim 2 \times 10^4$, we can use a straightforward Monte Carlo procedure, which of course benefits from the fact that node configurations are independent random variables when $n = 1$. Very large sizes require a more efficient "knitting" procedure.

In the straightforward approach, we construct independent $L \times L$ samples, assigning the node configurations at random

with the probabilities in Sec. II A. By following the loops, we then calculate the spanning number n_s, the loop length distribution, $P(l)$, the average linear size of a loop of length l, $\Delta X(l)$, and the correlation functions G_2 and G_4 at separation $L/2$. The spanning number (defined in Sec. IV B) requires open cylinder boundary conditions, while fully periodic BCs are used for the other observables. However, the same samples may be used for both, since the Boltzmann weight is independent of the boundary conditions when $n = 1$.

The two-leg correlator $G_2(L/2)$ is the probability that two links at separation $L/2$ lie on the same loop, and we take $G_4(L/2)$ to be the probability that two nodes at separation $L/2$ are visited by the same pair of loops. This is not the only way that two nodes can be joined by four strands—the four strands can make up a single loop rather than a pair—but the scaling is the same for the two types of contribution.

The data for $P(l)$ and $\Delta X(l)$ are stored in histograms in a logarithmic scale in l. For each box we calculate the mean and standard deviation of the loop size. The former gives the estimate of $\Delta X(l)$; to avoid finite size effects, a box is discarded if its ΔX is within two standard deviations of L. With this procedure, the number of independent samples constructed for a given system size varied between 2×10^5 for the largest size and 2×10^6 for the smallest.

A. Knitting

As we expect logarithmic behavior in the Goldstone phase, it is crucial to be able to study very large systems. The straightforward procedure above is very efficient in terms of CPU time, but it is limited by the available computer memory since it requires us to store the full configuration. The first improvement comes from the fact that a cylinder of circumference L can be "knitted" by the successive addition of $L \times L'$ strips, where L' is of order one.

At a given stage in the growth of the cylinder, it contains both closed loops in the interior, and strands that end on the boundary. The lengths and sizes of the closed loops are already included in the histograms for $P(l)$ and $\Delta X(l)$. Then, the only information about the configuration that we need to store is the connectivity of the links on the boundary, together with the lengths of the connecting strands. (Note that this connectivity information is configuration-dependent—this is distinct from the transfer matrix approach, in which the transfer matrix is not configuration dependent and which is limited to small sizes.) When we add a new strip to the cylinder some loops will become closed: we add their lengths l and their sizes ΔX—defined as the height of the loop in the growing direction—to our histograms.

Growing the cylinder strip by strip, the required memory is proportional to the circumference L (strictly to $L \ln L$) rather than to L^2 as in the straightforward approach (algorithms for percolation which avoid storing the full configuration also exist[60]). We have been able to compute cylinders with L up to 10^6 and height much greater than L.

This method requires storing the (realization-dependent) connectivity information for the boundary links of a large cylinder. This has the flavor of a transmission matrix in a localization problem. In the future it would be interesting to consider the properties of this "matrix" in more detail.

B. Shuffling

A further improvement that significantly reduces CPU effort involves constructing sets of strips of width L and height $H = L/20$ (using the knitting procedure). For each strip, we store the connectivity of the boundary links. Joining 20 of them yields a square sample, and we have enough information about this sample to calculate $G_2(x,y)$ (for links x and y which lie on the boundaries of two strips) as well as n_s. From each set of 20 pieces, many different samples may be created by shuffling the order of the pieces and by rotating them in the transverse direction. We construct 1000 samples for each set. These samples are not of course independent, so we estimate error bars by producing many independent such sets (80–200) and examining the statistical fluctuations between sets.

For the calculation of n_s in large systems to a given precision, the shuffling and rotation of strips reduces CPU time by a factor of 200. We have parallelized this procedure for OpenMP and for CUDA GPUs. The parallelization for the graphics cards was particularly efficient—a typical program ran almost 100 times faster on an Nvidia Tesla M2070 card than on a single core in an Intel Xeon E5520 CPU.

VII. POLYMER COLLAPSE

A long polymer with repulsive (or excluded volume) interactions between segments displays the universal behavior of the lattice self-avoiding walk (SAW), while strong enough attractive interactions cause the polymer to collapse. The boundary between these two regimes is the so-called Θ point. In de Gennes' description of the polymer via the $O(N \to 0)$ model, the SAW corresponds to the critical point, and the Θ point to the tricritical point.[1,43,61] However, the actual situation is more complicated, especially in two dimensions.

While the SAW behavior is extremely robust, the Θ point is more subtle. Different lattice models can yield different universality classes of collapse transition,[16,18,62,63] and it also turns out that the phase diagram in the vicinity of the Θ point can have a more complex structure than would naively have been expected.[18,62,64,65]

The interacting self-avoiding trail model (ISAT) has been particularly controversial,[16,18,24,66–68] with numerous conflicting results and hypotheses put forward for the critical exponents at the collapse point. In this model, the polymer can visit links only once, but nodes twice, so allowed configurations of a closed polymer are equivalent to allowed configurations of a single loop in the CPLC. Here, we give a field theoretic description of the ISAT which explains the phase diagram found numerically[18] and shows that the ISAT Θ point is highly fine-tuned from the point of view of more general polymer models, being an infinite-order multicritical point at which the $O(N)$ symmetry of the problem is enhanced from the generic $O(N \to 0)$ to $O(N \to 1)$.

On a lattice of large finite size L, the ISAT partition function is[69]

$$Z_{\rm pol}(k,t) = \sum_{\substack{\text{polymer}\\ \text{configs}}} k^{\text{length}} t^{\text{no. self-contacts}}. \qquad (65)$$

A self-contact is a node visited twice by the polymer. We are now at fixed length fugacity rather than fixed length, but the

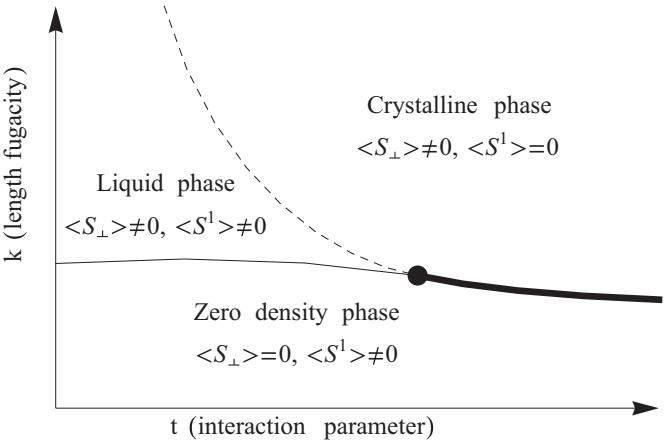

FIG. 16. Schematic representation of the phase diagram for the polymer found in Ref. 18, together with our interpretation in terms of a perturbed $O(1+n')$ model in the limit $n' \to 0$. The thin solid line is in the universality class of the self-avoiding walk (polymer in good solvent). The dot is the multicritical collapse point, or Θ point, with full $O(1+n')$ symmetry. The bold line is a first-order transition. The dashed line is a transition in the Ising universality class between two regimes in which the polymer is dense (visits a finite fraction of the links of the lattice): the "crystalline" and "liquid" phases.

two ensembles are simply related.[70] The parameter t controls interactions which are repulsive for $t < 1$ and attractive for $t > 1$.

An interesting feature of this model is the phase diagram, obtained numerically by Foster.[18] A schematic version is shown in Fig. 16. For small k, the polymer is of finite typical size and not critical (the zero-density phase), while for large k it is dense, i.e., has length of order L^2. When t is small, the transition between these phases shows the usual critical behavior of the SAW (thin solid line), and for large t there is a first-order transition associated with the collapsed polymer (thick line). The Θ point separates these.

An unexpected feature, from the point of view of the de Gennes theory, is an additional line of transitions within the dense phase (dashed line), which are found numerically to be in the Ising universality class.[18] A similar line of Ising transitions terminating at a Θ point was found in a polymer model without crossings studied by Blöte and Nienhuis,[62] and a heuristic explanation was provided by associating Ising degrees of freedom with the faces of the lattice,[62,71] for which the polymer was a domain wall. In that model, the absence of crossings also allows for a Coulomb gas description that captures the Ising transition.[72]

For a field-theoretic description of the ISAT, we make use of the fact that precisely at the Θ point, which is at $k = 1/3$, $t = 3$,[16] the ISAT maps to the CPLC at a point in the Goldstone phase, namely $n = 1$, $p = 1/3$, $q = 1/2$. The Θ point is therefore described by the $O(n \to 1)$ σ model,[10] and we can understand the region around it by perturbing this σ model. The following considerations may readily be generalized to the various modifications of ISAT that have been studied numerically, e.g., on other lattices,[64] with additional interactions,[73–75] or in higher dimensions.[76]

Before continuing, we note that an alternative conjecture for the critical behavior of the ISAT Θ point was put forward on the basis of numerical transfer matrix calculations in Ref. 18. According to this conjecture, the Θ point has nontrivial critical exponents identical to those of an exactly solvable model of polymers *without* intersections.[62,77] This is at odds with the predictions of the Goldstone phase, which yields trivial critical exponents together with universal logarithmic corrections. We believe the Goldstone phase scenario is convincingly established by our numerical results for large systems (note that Sec. IV B includes data at the relevant point $p = 1/3$, $q = 1/2$), together with the logarithmic behavior seen numerically in Refs. 16 and 17 and the theoretical arguments of Ref. 10 and Sec. III, and that the apparent nontrivial exponents in Ref. 18 are due to logarithmic finite size corrections (see the endnote[78] for more details).

To describe the single-polymer problem in the language of the spin model, we proceed along similar lines to Sec. IV C, expanding the partition function for the CPLC in $n' = n - 1$ to separate out configurations with a single marked loop (which will be our polymer).

To control k and t for this polymer, we must modify the partition function (24) in a way that breaks the symmetry of the $O(n)$ σ model down to $\mathbb{Z}_2 \times O(n')$. At each node, Eq. (24) contains terms of the form $(\vec{S}_1 \cdot \vec{S}_2)(\vec{S}_3 \cdot \vec{S}_4)$. Such a term corresponds to two sections of loop passing through the node, one connecting link 1 to link 2, and one connecting link 3 to link 4. In the new ensemble, these sections can be sections of marked or unmarked loops, and we modify the weights accordingly:

$$\begin{aligned}(\vec{S}_1 \cdot \vec{S}_2)(\vec{S}_3 \cdot \vec{S}_4) \quad \longrightarrow \quad & \left(S_1^1 S_2^1\right)\left(S_3^1 S_4^1\right) + 3k\left(S_1^1 S_2^1\right)(\vec{S}_{\perp 3} \cdot \vec{S}_{\perp 4}) \\ & + 3k(\vec{S}_{\perp 1} \cdot \vec{S}_{\perp 2})\left(S_3^1 . S_4^1\right) \\ & + 3k^2 t\,(\vec{S}_{\perp 1} \cdot \vec{S}_{\perp 2})(\vec{S}_{\perp 3} \cdot \vec{S}_{\perp 4}). \end{aligned} \tag{66}$$

Each unit of marked length acquires a factor of $3k$, and each meeting of two marked strands acquires an additional factor of $t/3$. Expanding in n' as in Eqs. (43) and (45),

$$Z(n',k,t) = 1 + n' \sum_{\substack{\mathcal{C};\text{ one} \\ \text{marked loop}}} W_{\mathcal{C}}\,(3k)^{\text{length}}(t/3)^{\text{no. self-contacts}} + \cdots .$$

Separating the sum into a sum over configurations of the marked loop (polymer) and a sum over the configurations of the other loops, and performing the latter,

$$Z(n',k,t) = 1 + n'\,Z_{\text{pol}}(k,t) + \cdots . \tag{67}$$

We discuss only the partition function, but one may easily check that the natural geometrical correlation functions in the polymer problem, i.e., the watermelon correlators, can be expressed as correlators of $\vec{S}_\perp$ in the replica limit $n' \to 0$.

The polymer multicritical point at $(k,t) = (\frac{1}{3},3)$ corresponds to the CPLC at $p = 1/3$, $q = 1/2$ and therefore to the σ model with full $O(n)$ symmetry. Varying (k,t) away from this point introduces symmetry-breaking perturbations, of which the most relevant are γ_1 and γ_2:

$$\begin{aligned} \mathcal{L} &= \frac{K}{2}[(\nabla \vec{S})^2 + \gamma_1 O_{\perp 1} + \gamma_2 O_{\perp 2}], \\ O_{\perp 1} &= \vec{S}_\perp^2, \quad O_{\perp 2} = (\vec{S}_\perp^2)^2 - \frac{2(n+1)}{n+4} S_\perp^2. \end{aligned} \tag{68}$$

Before considering the more detailed RG picture, we identify the phases in Fig. 16 with the phases of this perturbed σ model. These are characterized by whether the $\mathbb{Z}_2$ and $O(n')$ symmetries are broken, i.e., whether $\langle S^1\rangle \neq 0$ and whether $\langle \vec{S}_\perp\rangle \neq 0$.

When $\langle \vec{S}_\perp\rangle \neq 0$, the polymer fills the system densely and the transverse modes $\vec{S}_\perp$ are in a Goldstone phase. To see that such a phase is possible, note that when fluctuations in S^1 are massive, we may imagine integrating them out to get an effective $O(n')$ σ model for $\vec{S}_\perp$. In the limit $n' \to 0$, this σ model has a Goldstone phase as a consequence of the β function in Eq. (23). This is just the theory for the dense polymer with crossings studied in Ref. 10.

The phase with $\langle S^1\rangle = \langle \vec{S}_\perp\rangle = 0$ does not appear upon perturbing around the Θ point, since the latter is controlled by the fixed point at infinite stiffness. However, the other three do.

(1) Zero-density phase, $\langle \vec{S}_\perp\rangle = 0$, $\langle S^1\rangle \neq 0$. The leading effect of reducing the length fugacity k below the Θ-point value is to introduce a mass for $\vec{S}_\perp$, so that $\vec{S}$ orders in the longitudinal direction and the transverse modes $\vec{S}_\perp$ are massive. Correlators thus decay exponentially for the polymer, and it has a finite typical size.[79]

(2) Dense phase with Ising disorder, $\langle \vec{S}_\perp\rangle \neq 0$ & $\langle S^1\rangle = 0$. Moving away from the Θ point by increasing k makes S^1 massive, and $\vec{S}$ "orders" in the transverse plane. The system thus goes from the Goldstone phase of the $O(n \to 1)$ model to the Goldstone phase of the $O(n \to 0)$ model. The two-leg watermelon correlation function is a constant at long distances, as discussed in Sec. IV A, meaning that the polymer is dense.

(3) Dense phase with Ising order, $\langle \vec{S}_\perp\rangle \neq 0$ and $\langle S^1\rangle \neq 0$. For appropriate values of the coefficients γ_1, γ_2, the renormalized free energy is minimized when both $\langle \vec{S}_\perp\rangle$ and $\langle S^1\rangle$ are nonzero, so that both symmetries, $\mathbb{Z}_2$ and $O(n')$, are broken.

[A minor subtlety regarding the above classification is that only gauge-invariant operators are meaningful in the loop model/$\mathbb{RP}^{n-1}$ model. For this reason, the global symmetry of the perturbed loop model[80] is $O(n') = \mathbb{Z}_2 \times SO(n')$, rather than $\mathbb{Z}_2 \times O(n')$ as in the perturbed $O(n)$ σ model. However, we are free to use the language of the latter, which (for the reasons discussed in Sec. III D) captures the universal properties of the perturbed $\mathbb{RP}^{n-1}$ σ model in the regime we are considering.]

The field theory description also determines the nature of the phase transitions. First, consider the thin solid line in Fig. 16. The field S^1 is Ising-ordered on both sides of this transition, and its massive fluctuations play no role in the critical behavior of $\vec{S}_\perp$. We therefore have the critical point of the $O(n')$ model in the limit $n' \to 0$. This is the usual description of the self-avoiding walk,[1,43] confirming what we expect and find in the polymer problem.

Next, consider the dashed line in Fig. 16. Here, S^1 undergoes an ordering transition at which $\mathbb{Z}_2$ symmetry is broken. Thus we would expect an Ising transition. We must check, however, that the massless degrees of freedom associated with $\vec{S}_\perp$—which are in the Goldstone phase—do not modify the Ising critical behavior. But it is easy to see they do not. The most relevant coupling allowed by $\mathbb{Z}_2 \times O(n')$ symmetry is via the product of the energy operators,

$$E_{\text{Ising}} \times E_{\text{Goldstone}}. \tag{69}$$

This composite operator has dimension $(\text{length})^{-3}$, so is irrelevant.

Finally, consider the thick line in the figure, which separates phases breaking different symmetries [$\mathbb{Z}_2$ on one side, and $O(n')$ on the other]. According to Landau theory, this transition should be first order, as it is numerically found to be.[18]

What does Ising order/disorder mean for the polymer? Define a new configuration of Ising spins μ_F on the faces F of the square lattice by the requirement that the polymer is the (only!) domain wall in this configuration. Then the dense phase with Ising *disorder* corresponds to antiferromagnetic *order* in μ, while μ is disordered in the dense phase with Ising order. (To show this, we write $\langle \mu_F \mu_{F'}\rangle$ in terms a correlator of twist fields in the $\mathbb{RP}^{n-1}$ model, which force the fields Q^{1a} with $a > 1$ to change sign on a line connecting F and F'.) Antiferromagnetic order in μ is equivalent to the crystalline order of Ref. 18, and it becomes perfect when the polymer visits every link of the lattice. It is also essentially equivalent to the Ising order defined in Refs. 62 and 71 for a different model.

For a more detailed picture of the phase diagram, we use the RG equations for the σ model. We must include the lowest two anisotropies as in Eq. (68), where γ_1, γ_2 are linearly related to the perturbations

$$\delta k = k - 1/3, \quad \delta t = t - 3 \tag{70}$$

when these are small (we will give approximate expressions below). After running the RG up to a large time τ_*, we have (for $n = 1$)

$$K_* \sim \frac{\tau_*}{2\pi}, \quad \gamma_{1*} \sim \frac{\gamma_1 e^{2\tau_*}}{(\tau_*/2\pi K)^2}, \quad \gamma_{2*} \sim \frac{\gamma_2 e^{2\tau_*}}{(\tau_*/2\pi K)^7}.$$

For generic small initial values (γ_1, γ_2), we will renormalize to a regime where $\gamma_{1*} = O(1)$ and $|\gamma_{2*}| \ll |\gamma_{1*}|$, putting us deep within one of the phases—either the zero-density phase or the dense phase with Ising disorder, depending on the sign of γ_1. The phase transitions occur instead in the regime where the renormalized γ_{1*} and γ_{2*} become of order one simultaneously.

Since the stiffness of the renormalized σ model is large ($\tau_* \sim \ln|\gamma_1|^{-1/2} \sim \ln|\gamma_2|^{-1/2}$), we may determine which phase it is in simply by minimizing the potential in the renormalized Lagrangian. In doing this, we must bear in mind the constraint $\vec{S}^2 = 1$. We find the three phases described above, with the phase transition lines located at

$$\text{SAW:} \quad \gamma_1 \simeq \frac{4}{5}\gamma_2 \left(\frac{4\pi K}{\ln 1/|\gamma_2|}\right)^5 \qquad (\gamma_2 > 0),$$

$$\text{Ising:} \quad \gamma_1 \simeq -\frac{3}{5}\gamma_2 \left(\frac{4\pi K}{\ln 1/|\gamma_2|}\right)^5 \qquad (\gamma_2 > 0),$$

$$\text{1storder:} \quad \gamma_1 \simeq -\frac{1}{5}\gamma_2 \left(\frac{4\pi K}{\ln 1/|\gamma_2|}\right)^5 \qquad (\gamma_2 < 0).$$

(These formulas are valid asymptotically close to the Θ point.) For a very crude estimate of the relation between (γ_1, γ_2) and

$(\delta k, \delta t)$, we can evaluate the right-hand side of Eq. (66) for spatially constant $\vec{S}_l$, and take the logarithm of the Boltzmann weight for a node to obtain the potential terms in the bare Lagrangian. We find

$$\gamma_1 \sim -C\left(\delta k + \frac{2}{45}\delta t\right), \quad \gamma_2 \sim -C\frac{\delta t}{18}, \tag{71}$$

where C is an undetermined constant. The above confirms that the three phases meet at the Θ point, and shows that the SAW and Ising critical lines are asymptotically parallel as they approach the Θ point.

A remarkable consequence of the above field theory mapping is that the Θ point of the ISAT—despite the simplicity and naturalness of this model—is in fact an infinite order multicritical point! We have mentioned the two most relevant anisotropies $O_{\perp 1}$ and $O_{\perp 2}$, but there is an infinite number of these, with $O_{\perp k} = (S_\perp^2)^k + \cdots$, and generic perturbations of the ISAT Θ point will introduce all of them with couplings γ_k. At $n = 1$, the RG equation for γ_k is

$$\frac{\mathrm{d}\gamma_k}{\mathrm{d}\tau} = \left(2 - \frac{2k^2 - k + 1}{2\pi K}\right)\gamma_k + \cdots, \tag{72}$$

so they are all relevant at the $K = \infty$ fixed point.

The Θ point of the ISAT does not therefore represent the universality class of the *generic* Θ point polymer model with crossings. (This explains why the model in Ref. 82 shows different behavior to the ISAT.) A similar argument explains why the three-dimensional ISAT[76] shows distinct universal behavior from standard models of polymer collapse.

In two dimensions, the generic Θ-point behavior in the presence of crossings is different from that[63] in their absence. Since the ISAT Θ point does not represent the generic behavior of the Θ-point polymer with crossings [which we expect to be described by the tricritical $O(N \to 0)$ model], the exact exponents for the latter are still unknown. We will discuss RG flows for Θ-point polymers in detail in a separate publication.

VIII. OUTLOOK

The loop models we have discussed are described by "replica" σ models of the kind familiar from localization and polymer physics. Such problems remain at the frontier of our understanding of critical phenomena, and we hope that the transitions in the loop models will provide a testing ground for new approaches.

While exact results for the critical behavior discussed in Sec. V would be desirable, the development of more accurate analytical approximations would also be enlightening. On the numerical side,[81] work on the critical loop model should be extended to other values of n, either via Monte Carlo or the transfer matrix,[23] in order to pin down the properties of the whole family of critical points for $0 < n < 2$. We plan to return to these issues. (Three-dimensional $\mathbb{RP}^{n-1}$ loop models exist as well—we will report numerical results elsewhere.)

The connection between the CPLC at $n = 1$ and disordered fermions remains an open question. To begin with, recall the situation for the loop model without crossings ($p = 0$). This can be related to localization in at least two ways. Firstly, a limiting case of the Chalker Coddington model for the quantum Hall effect,[83] in which the scattering matrices at a node become "classical," yields the loop model without crossings, i.e., classical percolation. This is the familiar semiclassical description of the quantum Hall transition,[84] but because quantum tunneling has not been taken into account, it does not correctly capture the universal critical behavior. However, the loop model has a second relationship with localization, which is less obvious and which does not rely on suppressing quantum tunneling. This is due to an exact mapping from a network model for the spin quantum Hall transition (an analog of the quantum Hall transition, but in symmetry class C rather than A) to the loop model.[26–28,32]

For loops with crossings ($p > 0$) we can again construct a mapping of the first kind by taking a classical limit in a network model with a Kramers doublet on each edge (replacing each quantum node with one of the three classical possibilities in Fig. 2). However, this correspondence is rather trivial because of the explicit suppression of quantum tunneling. It would be interesting to know whether the analogy with localization goes beyond this—in particular, whether the critical behavior of the loop model can be related to the critical behavior of a true localization problem. (It is interesting to note that our value of ν is close to estimates of ν for the symplectic class.[85])

Returning to loop models in their own right, there is a good understanding of the zoology of critical points in loop models without crossings, many of which fit into the one-parameter family of universality classes in SLE_κ. In general, crossings take us outside this family. Here we have discussed a new line of critical points exemplifying this, but we certainly do not expect that this exhausts the possibilities for new critical behavior—much remains to be learned.

ACKNOWLEDGMENTS

We are very grateful to J. Chalker for many useful discussions and for valuable comments on the manuscript. AN also thanks L. Fu, J. Jacobsen, L. Jaubert, A. Ludwig, T. Prellberg, K. Shtengel, and especially, J. Cardy and F. Essler for useful discussions, and B. Nienhuis for correspondence. PS, AMS, and MO acknowledge financial support from the Spanish DGI and FEDER, Grants No. FIS2012-38206 and No. AP2009-0668. This work was supported in part by the EPSRC.

[1] P. G. de Gennes, Phys. Lett. A **38**, 339 (1972).
[2] G. Parisi and N. Sourlas, J. Phys. Lett. **41**, 403 (1980).
[3] A. J. McKane, Phys. Lett. A **76**, 22 (1980).
[4] A. M. M. Pruisken, Nucl. Phys. B **235**, 277 (1984).
[5] H. Levine, S. B. Libby, and A. M. M. Pruisken, Phys. Rev. Lett. **51**, 1915 (1983).
[6] H. Weidenüller, Nucl. Phys. B **290**, 87 (1987).
[7] F. Evers and A. D. Mirlin, Rev. Mod. Phys. **80**, 1355 (2008).

[8]P. Fendley, in *New Theoretical Approaches to Strongly Correlated Systems*, edited by A. M. Tsvelik (Kluwer, Dordrecht, 2001) [arXiv:cond-mat/0006360].
[9]C. Candu, J. L. Jacobsen, N. Read, and H. Saleur, J. Phys. A **43**, 142001 (2010).
[10]J. L. Jacobsen, N. Read, and H. Saleur, Phys. Rev. Lett. **90**, 090601 (2003).
[11]N. Read and H. Saleur, Nucl. Phys. B **613**, 409 (2001).
[12]A. Nahum and J. T. Chalker, Phys. Rev. E **85**, 031141 (2012).
[13]A. Nahum, J. T. Chalker, P. Serna, M. Ortuño, and A. M. Somoza, Phys. Rev. Lett. **107**, 110601 (2011).
[14]B. Nienhuis, in *Phase Transitions and Critical Phenomena*, edited by C. Domb and J. Liebowitz (Academic Press, Singapore, 1987), Vol. 11, Chap. 1.
[15]J. Cardy, Ann. Phys. **318**, 81 (2005).
[16]A. L. Owczarek and T. Prellberg, J. Stat. Phys. **79**, 951 (1995).
[17]R. M. Ziff, X. P. Kong, and E. G. D. Cohen, Phys. Rev. A **44**, 2410 (1991).
[18]D. P. Foster, J. Phys. A: Math. Theor. **42**, 372002 (2009).
[19]E. J. Konig, P. M. Ostrovsky, I. V. Protopopov, and A. D. Mirlin, Phys. Rev. B **85**, 195130 (2012).
[20]L. Fu and C. L. Kane, Phys. Rev. Lett. **109**, 246605 (2012).
[21]M. J. Martins, B. Nienhuis, and R. Rietman, Phys. Rev. Lett. **81**, 504 (1998).
[22]W. Kager and B. Nienhuis, J. Stat. Mech. (2006) P08004.
[23]Y. Ikhlef, J. Jacobsen, and H. Saleur, J. Stat. Mech. (2007) P05005.
[24]J. W. Lyklema, J. Phys. A: Math. Gen. **18**, L617 (1985)
[25]J. Cardy, J. Phys. A: Math Gen. **34**, L665 (2001).
[26]I. A. Gruzberg, A. W. W. Ludwig, and N. Read, Phys. Rev. Lett. **82**, 4524 (1999).
[27]E. J. Beamond, J. Cardy, and J. T. Chalker, Phys. Rev. B **65**, 214301 (2002).
[28]A. D. Mirlin, F. Evers, and A. Mildenberger, J. Phys. A: Math. Gen. **36**, 3255 (2003).
[29]M. Ortuño, A. M. Somoza, and J. T. Chalker, Phys. Rev. Lett. **102**, 070603 (2009).
[30]Y. Ikhlef, P. Fendley, and J. Cardy, Phys. Rev. B **84**, 144201 (2011).
[31]E. Bettelheim, I. A. Gruzberg, and A. W. W. Ludwig, Phys. Rev. B **86**, 165324 (2012).
[32]J. Cardy, in *50 Years of Anderson Localization*, edited by E. Abrahams (World Scientific, Singapore, 2010).
[33]V. Gurarie, Nucl. Phys. B **410**, 535 (1993).
[34]A. Gainutdinov, J. L. Jacobsen, N. Read, H. Saleur, and R. Vasseur, arXiv:1303.2082 (2013); J. Cardy, arXiv:1302.4279 (2013); V. Gurarie, arXiv:1303.1113 (2013).
[35]T. Senthil, M. P. A. Fisher, L. Balents, and C. Nayak, Phys. Rev. Lett. **81**, 4704 (1998); R. Bundschuh, C. Cassanello, D. Serban, and M. R. Zirnbauer, Phys. Rev. B **59**, 4382 (1999).
[36]T. Senthil, J. B. Marston, and M. P. A. Fisher, Phys. Rev. B **60**, 4245 (1999).
[37]E. J. Beamond, A. L. Owczarek, and J. Cardy, J. Phys. A: Math. Gen. **36**, 10251 (2003).
[38]J. M. F. Gunn and M. Ortuño, J. Phys. A: Math. Gen. **18**, L1095 (1985).
[39]K. Shtengel and L. P. Chayes, J. Stat. Mech. (2005) P07006.
[40]J. T. Chalker, M. Ortuño, and A. M. Somoza, Phys. Rev. B **83**, 115317 (2011).
[41]N. Read and H. Saleur, Nucl. Phys. B **777**, 263 (2007).
[42]E. Domany, D. Mukamel, B. Nienhuis, and A. Schwimmer, Nucl. Phys. B **190**, 279 (1981).
[43]J. Cardy, *Scaling and Renormalization in Statistical Physics* (Cambridge University Press, Cambridge, 1996).
[44]N. D. Mermin, Rev. Mod. Phys. **51**, 591 (1979).
[45]P. E. Lammert, D. S. Rokhsar, and J. Toner, Phys. Rev. Lett. **70**, 1650 (1993).
[46]Otherwise, there can be flux through holes or handles of the manifold. In the graphical expansion, the sum over the resulting flux sectors is responsible for killing loop configurations which do not correspond to percolation configurations.
[47]However, at this special value of q, we can define k-leg operators for odd k by taking $O_k = S'^1 \dots S'^k$.
[48]S. Hikami, Phys. Lett. B **208**, 98 (1981).
[49]E. Fradkin, *Field Theories of Condensed Matter Physics*, 2nd ed. (Cambridge University Press, Cambridge, 2013).
[50]One way to show this explicitly is to map an anisotropic version of the loop model to a quantum spin chain with next-nearest-neighbor couplings, which can be coarse-grained using standard techniques.
[51]I. Affleck, Phys. Rev. Lett. **56**, 408 (1986).
[52]T. Senthil and M. P. A. Fisher, Phys. Rev. B **74**, 064405 (2006).
[53]A. M. Polyakov, Phys. Lett. B **59**, 79 (1975).
[54]Loops in the interior and curves with both ends on the same boundary both retain fugacity n—for example, a curve with both ends on the upper boundary can either be of color $a = 1$, in which case it has weight $n\cos^2\theta$, or of color $a = 2$, when it has weight $n\sin^2\theta$, and the sum gives n. Spanning curves on the other hand must be of color $a = 1$ and have weight $n\cos\theta$.
[55]In the mapping of Sec. III E, this sign comes from factors of $\vec{S}_{\rm top}\cdot\vec{S}_l$ and $\vec{S}_{\rm bottom}\cdot\vec{S}_l$ in the Boltzmann weight for links l adjacent to the boundary links.
[56]R. A. Pelcovits and D. R. Nelson, Phys. Lett. A **57**, 23 (1976); D. R. Nelson and R. A. Pelcovits, Phys. Rev. B **16**, 2191 (1977).
[57]J. Cardy, in *Fluctuating Geometries in Statistical Mechanics and Field Theory*, edited by F. David, P. Ginsparg, and J. Zinn-Justin (Elsevier, 1998).
[58]For $n > 2$, a $\mathbb{Z}_2$ vortex corresponds to, e.g., $\vec{S} = (\cos\theta/2, \sin\theta/2, 0, \dots, 0)$; note that when $n = 2$, this configuration becomes a $\mathbb{Z}$ vortex of charge ± 1. (Here, θ is a polar coordinate; recall $\vec{S} \sim -\vec{S}$.)
[59]J. L. Cardy and H. W. Hamber, Phys. Rev. Lett. **45**, 499 (1980).
[60]J. Hoshen and R. Kopelman, Phys. Rev. B **14**, 3438 (1976).
[61]P. G. de Gennes, J. Phys. Lett. **36**, 55 (1975).
[62]H. W. J. Blöte and B. Nienhuis, J. Phys. A: Math. Gen. **22**, 1415 (1989).
[63]B. Duplantier and H. Saleur, Phys. Rev. Lett. **59**, 539 (1987).
[64]J. Doukas, A. L. Owczarek, and T. Prellberg, Phys. Rev. E **82**, 031103 (2010).
[65]W. Guo, H. J. Blöte, and B. Nienhuis, Int. J. Mod. Phys. C **10**, 301 (1999).
[66]A. Guha, H. A. Lim, and Y. Shapir, J. Phys. A: Math. Gen. **21**, 1043 (1988).
[67]H. Meirovitch and H. A. Lim, Phys. Rev. A **38**, 1670 (1988).
[68]Y. Shapir and Y. Oono, J. Phys. A: Math. Gen. **17**, L39 (1984).
[69]Translated versions of a loop are counted as distinct polymer configurations in the above sum.
[70]Fixed length fugacity k is more convenient from the point of view of field theory and also if we wish to consider phases in which the polymer becomes space filling. The two ensembles are related by a Laplace transform. The critical properties of a polymer of fixed large length on an infinite lattice are governed by the singularity of

the partition function closest to $k = 0$,[43] i.e., in the case of Fig. 16 by a point on the line separating the zero-density phase from the dense phase. The crystalline and liquid phases are dense, i.e., the length of the polymer is comparable with the lattice area.

[71] H. W. J. Blöte, M. T. Batchelor, and B. Nienhuis, Physica A **251**, 95 (1998).

[72] J. L. Jacobsen and J. Kondev, J. Stat. Phys **96**, 21 (1999).

[73] A. Bedini, A. L. Owczarek, and T. Prellberg, Physica A **392**, 1602 (2013); Phys. Rev. E **87**, 012142 (2013).

[74] D. P. Foster, Phys. Rev. E **84**, 032102 (2011).

[75] D. P. Foster, J. Phys. A: Math. Theor. **43**, 335004 (2010).

[76] T. Prellberg and A. L. Owczarek, Phys. Rev. E **51**, 2142 (1995); A. Bedini, A. L. Owczarek, and T. Prellberg, *ibid.* **86**, 011123 (2012).

[77] S. O. Warnaar, M. T. Batchelor, and B. Nienhuis, J. Phys. A: Math. Gen. **25**, 3077 (1992).

[78] We can use the σ model to estimate the eigenvalues of the transfer matrix for a cylinder of circumference L. Coarse-graining by a factor L yields an effective 1D σ model with renormalized stiffness $\tilde{K}_L$. This is equivalent to the quantum mechanics of a particle on an $(n-1)$-dimensional sphere, with energy levels $E_k = k(k-1)/(2\tilde{K}_L)$, $k = 0,1,2,\ldots$ in the limit $n \to 1$. This leads to the finite size estimates $x_k = E_k/2\pi$ for the scaling dimensions, which tend to zero logarithmically with L. For a very crude estimate at small sizes, we can approximate $\tilde{K}_L$ by the spanning number on an $L \times L$ cylinder, which we have calculated numerically at $p = 1/3$. For L from 5 to 12, this gives x_2 varying from 0.103 to 0.086.

[79] In the zero-density phase, the unmarked loops remain in the Goldstone phase, being unaffected by the polymer since it is short. In order to write down watermelon correlation functions for the unmarked loops, we would have to extend S^1 to a vector $\vec{S}_1$ with $m \to 1$ components, increasing the symmetries of the field theory to $O(m) \times O(n')$.

[80] The zero-density phase breaks no symmetries of the perturbed $\mathbb{RP}^{n-1}$ model, the "dense phase with Ising order" fully breaks $O(n')$, and the "dense phase with Ising disorder" breaks only $\mathrm{SO}(n')$.

[81] The IPLC is also a candidate for numerical simulations: we expect universal behavior to coincide with that of the CPLC, but this remains to be confirmed.

[82] A. Bedini, A. L. Owczarek, and T. Prellberg, J. Phys. A **46**, 085001 (2013).

[83] J. T. Chalker and P. D. Coddington, J. Phys. C **21**, 2665 (1988).

[84] S. A. Trugman, Phys. Rev. B **27**, 7539 (1983).

[85] Y. Asada, K. Slevin, and T. Ohtsuki, Phys. Rev. Lett. **89**, 256601 (2002); P. Markos and L. Schweitzer, J. Phys. A **39**, 3221 (2006); A. Mildenberger and F. Evers, Phys. Rev. B **75**, 041303 (2007); H. Obuse, A. R. Subramaniam, A. Furusaki, I. A. Gruzberg, and A. W. W. Ludwig, *ibid.* **82**, 035309 (2010).